Methods to Detect Habitable Atmospheres on the Terrestrial Exoplanet TRAPPIST-1 e

by

D. Gatlin

Bachelor of Arts – Department of Astrophysical & Planetary Sciences

Undergraduate Honors Thesis

Defense Copy

Thesis Defense Committee:

Dr. Eric T. Wolf	Advisor	Atmospheric and Oceanic Sciences
Prof. Ann-Marie Madigan	Honors Council Representative	Astrophysical and Planetary Sciences
Prof. David Brain	External Faculty Member	Astrophysical and Planetary Sciences
Prof. Daniel Jones	External Faculty Member	Arts and Sciences Honors Program

To defend on:

2019–05–03

This thesis entitled:
Methods to Detect Habitable Atmospheres on the Terrestrial Exoplanet TRAPPIST-1 e
written by D. Gatlin
has been approved for the Department of Astrophysical and Planetary Science

Dr. Eric T. Wolf

Prof. Ann-Marie Madigan

Prof. David Brain

Prof. Daniel Jones

Date

The final copy of this thesis has been examined by the signatories, and we find that both the content and the form meet acceptable presentation standards of scholarly work in the above mentioned discipline.

Gatlin, D. (B.A., Astrophysics)

Methods to Detect Habitable Atmospheres on the Terrestrial Exoplanet TRAPPIST-1 e

Thesis directed by Dr. Eric T. Wolf

In order to better direct future exoplanetary research, we must be able to accurately predict what telescopes like the James Webb Space Telescope (JWST) will be able to detect. To this effect, NASA's Planetary Spectrum Generator (PSG) can be used to simulate observations, both during exoplanet transits and throughout an exoplanet's year. Such predictions allow us to make informed decisions about how to spend time on JWST and which techniques will allow for different types of analysis. In order to produce the most realistic results from the Planetary Spectrum Generator (PSG), self-consistent three-dimensional climate models of planets in the TRAPPIST-1 system are first used to simulate atmospheres on these tidally locked exoplanets, and understand how they might be different from the climate of Earth.

The TRAPPIST-1 exoplanets are assumed to be tidally locked with the host star. Recent climate modeling studies indicate that there are three distinct types of tidally locked exoplanet atmospheres; slow rotators, fast rotators, and an intermediate regime. Slow rotators have large substellar clouds that remain constant over time. Fast rotators will have a significant Coriolis force, resulting in much smaller substellar clouds and more intense zonal winds which advect clouds to the eastern side of the substellar point. In all cases, the thermal emission of a planet depends strongly on the spatial distribution of clouds, which would change from the perspective of a distant observer over the exoplanet's year.

I have constructed a data pipeline that uses climate models as inputs, then uses the PSG to produce spectra. This pipeline can use a number of climate models on a number of different planets to create transit spectra or thermal phase curves.

When studying terrestrial exoplanets, the most exiting cases are potentially habitable planets. The TRAPPIST-1 system is one of the most likely systems to host a habitable exoplanet.

TRAPPIST-1 e is the most likely habitable planet in the system. The most effective methods for JWST are the transit method and thermal phase curves. The transit method is the most widely used method for detecting exoplanets, and JWST will have high resolution spectrographs that will be able to detect many atmospheric species including CO_2 and H_2O. Additionally, accurate spectra may enable us to infer the surface temperature of a planet.

Transit spectra can tell us a lot about the terminator profile of an atmosphere, but it cannot tell us about other parts of the planet's surface. Transit spectra can also be prone to extinction by clouds or aerosols. Thermal phase curves will observe how the thermal emission of an exoplanet will change over the course of its year, and may be able to detect features like the nature of the substellar cloud, if a planet has entered a runaway greenhouse effect, or a snowball state. Thermal phase curves will look dramatically different for fast rotators like TRAPPIST-1 e compared to slow rotators, and these results can only be simulated with global circulation models used in conjunction with accurate radiative transfer models. Thermal phase curves are also very sensitive to the planet's temperature, and can therefore help determine if a planet is habitable. Future predictions for JWST should incorporate the results from global circulation models, and those models should be accurate to the exoplanets in question. Future observations should also consider thermal phase curves because they will be able to detect a range of different features than transit spectra and will enable us to more effectively understand potentially habitable terrestrial exoplanets.

Dedication

To my Grandpa, Dr. Terry Flanagan

1938 – 2018

Acknowledgements

Thank you to my family who helped encourage me on my way to becoming an astrophysicist. To my dad, my mom, and my sister, Mark, Erin, and Carolyn Gatlin. To my girlfriend, Grace Marshall.

Thank you to my advisors, Susan (Astromom) Armstrong and David Brain. To the professors I've worked alongside, Prof. Jeremy Darling and Prof. Seth Hornstein. To my research advisors, Prof. Guy Stringfellow and Dr. Eric Wolf.

Thank you to everyone who read my drafts, Prof. Donald Wilkerson and all my peers in PHYS 3050.

Thank you to my professors Prof. Zach Berta-Thompson, Prof. Nick Schneider, Prof. John Bally, Dr. Mathis Habich, Prof. Melissa Nigro, Prof. Jen Kay, Prof. Peter Pilewskie, and Prof. Alexandra Jahn. To my high school math teacher, Laurie Buchanan.

Thank you to my co-investigators, Dr. Eric Wolf, Dr. Ravi Kopparapu, Dr. Geronimo Villanueva, and Dr. Avi Mandell.

Facilities: Exoplanet Archive, Planetary Spectrum Generator

Contents

Tables

Table

Figures

Figure

Chapter 1

Introduction

Exoplanetary science is one of the most exciting fields in astrophysics. Until the Kepler mission, it was unknown how common exoplanets may be, but we have since estimated that approximately one third of all F, G, and K stars have at least one terrestrial exoplanet (Traub, 2012). Excitingly, we have found a number of terrestrial exoplanets which resemble Earth in mass, size, and most crucially, solar irradiance. These terrestrial exoplanets are the most likely candidates in the search for habitable worlds beyond Earth, and by extension, the most likely places to discover extraterrestrial life or a future home for humanity. To date, the list of exoplanets in the classical habitable zone is short, and few are close to Earth, but this will soon change with the recently launched Transiting Exoplanet Survey Satellite (TESS). TESS is expected to discover thousands of exoplanets smaller than Neptune and dozens of Earth sized planets, and was optimized for finding planets that are closer to Earth (Ricker et al., 2014). In conjunction with the James Webb Space Telescope (JWST), we expect to dramatically improve observations of potentially habitable worlds in nearby star systems.

The most easily detectable exoplanets orbit M-dwarfs, which are very low mass, dim stars. These exoplanets are likely tidally locked due to their close orbit to their host star (Turbet et al., 2018), meaning they don't rotate relative to their star. The solar system contains no example of such a planet; however, the Earth-Moon system does provide an example as the Moon is tidally locked to Earth. The atmospheres of tidally locked planets behave differently from any atmosphere we are previously familiar with, so the only way to characterize their atmospheres is via global circulation

models (GCMs). GCMs were invented to predict weather or climate change, and have proven scientifically valuable for a number of different planets throughout the solar system (Way et al., 2018). Many astronomers have made predictions of what JWST will see on exoplanets, but most of these predictions assume that habitable exoplanet atmospheres will be replicas of Earth (Fortney et al., 2018). However, recent 3D climate modeling experiments demonstrate that exoplanets are typically very different than Earth. For example, an exoplanet that receives approximately the same amount of sunlight as Earth, TRAPPIST-1 d, is less likely to be habitable than TRAPPIST-1 e, a planet that receives only 60% of the solar irradiance of Earth (Wolf, 2018).

With the launch of JWST on the horizon, it is essential that we know what to expect from observations, and atmospheric models are the best method for constraining predictions. Simply assuming a tidally locked exoplanet will appear identical to Earth is unreasonable and can lead to inaccurate conclusions. Using GCM simulations for planets in the TRAPPIST-1 system, we can self-consistently predict what the TRAPPIST-1 exoplanets may look like with regards to cloud distributions, precipitation, and temperature. NASA's Planetary Spectrum Generator (PSG) can then be used to generate spectra for these climate models, giving us more accurate predictions of what JWST might be able to see (Villanueva et al., 2018). Using the PSG, we can determine which spectral features would be detectable with JWST and using signal to noise analysis, we will help the astrophysics community prioritize their time with JWST.

In addition to exoplanet transit spectra, GCMs allow us to study exoplanets using other methods, most notably thermal emission phase curves. A GCM provides global resolution of an exoplanet's surface and atmosphere, but only a small fraction of it can be probed via the transit method. The PSG can allow us to measure the thermal emission of the planet as it rotates relative to the Earth over its year. Thermal phase curves measure the change in thermal brightness of an exoplanet as it orbits its star, and can be variable over time. Thermal phase curves have the advantage of providing unique signals depending on the climate of the planet. This technique serves as the best method to resolve features like clouds on exoplanets, and by extension, we may infer details about the planet's climate. Thermal phase curves and transit spectra provide two very

unique methods of probing an exoplanet's atmosphere, and together, they will help JWST find habitable worlds beyond Earth.

In this thesis, I will calculate both transit spectra and thermal phase curves of several habitable zone exoplanets, particularly TRAPPIST-1 e. In the following section, Chapter 2, I will explain the fundamentals of exoplanet research and exoplanet observations, with an emphasis on the variables significant to thermal phase curves and transits. In Chapter 3, I will review climate models from Wolf (2017, 2018), and particularly focus on the terminator atmosphere profile and the global cloud patterns. I will compare fast rotators and slow rotators, which have dramatically different cloud patterns, and therefore different thermal phase curves. In Chapter 4, I will explain the data pipeline around the PSG and the PSG as a tool to simulate spectra. In Chapter 5, I will show transit spectra results, analyze their behavior, and identify and measure prominent features. In Chapter 6, I will do the equivalent analysis for thermal phase curves, and compare slow rotators thermal phase curves to fast rotators. In Chapter 7, I will compare the transit spectra and thermal phase curves, identifying their respective strengths and weaknesses.

Chapter 2

Background

Isaac Newton was the first person to consider the possibility of exoplanets (Newton, 1846). It requires little more than a simple understanding of the solar system and Newtonian physics to consider the possibility that other stars may host their own planets. Any planet orbiting any star must obey Newton's version of Kepler's 3rd law,

$$T^2 = \frac{4\pi^2}{\mathrm{G}\left(m_* + m_p\right)} a^3, \tag{2.1}$$

where T is the orbital period of the orbit, a is its semi-major axis, m_* is the mass of the star, and m_p is the mass of the planet. In addition, the small mass approximation where $m_* >> m_p$ simplifies equation 2.1 to

$$T^2 = \frac{4\pi^2}{\mathrm{G}m_*} a^3, \tag{2.2}$$

which we can solve, even if the mass of the planet is unknown. If the orbital period of an exoplanet and the mass of the host star are known; the planet's semi-major axis can be calculated. Using the semi-major axis, the planet's solar irradiance can be calculated with

$$S_p = \sigma T_*^4 \frac{r_*^2}{a^2}, \tag{2.3}$$

where S_p is the solar irradiance for the exoplanet. This value can be calculated using only a few data points, and can be compared to the solar irradiance of Earth ($\mathrm{S}_\oplus \approx 1361 \mathrm{W\,m^{-2}}$). A simple

narrative would be that if the $S_p \approx \mathrm{S}_\oplus$, then the planet is Earth-like. This understanding defined exoplanetary knowledge for hundreds of years, and technological limitations slowed further progress in our understanding of exoplanets.

The most naïve method for detecting an exoplanet is by direct imaging, just like we do for stars; however, the math behind this isn't very promising. If you approximate a planet as a blackbody, its flux is proportional to R^2T^4, then a 300 K exoplanet with a radius of $1\mathrm{R}_\oplus$ around a 3000 K star with a radius of 0.17 $R_\odot$ would be $^1/_{10{,}000{,}000^{\mathrm{th}}}$ as bright, which corresponds to a difference in 16 magnitudes. While observing two stars 16 magnitudes apart is certainly possible in optimal circumstances, it is virtually impossible to do when trying to view exoplanets because an exoplanet and its host star are almost always within the diffraction limit of each other. Telescopes large enough to detect an exoplanet have existed for over a hundred years, the primary limitation has always been the instrumentation.

This changed with the introduction of the CCD, which allowed for accurate photometry of dim objects in relatively short time periods. Astronomers are now able to detect exoplanets with a new method, instead of measuring the brightness of the planet, it is possible to measure the change in the brightness of the star. In 2003, the first exoplanet was detected by measuring the decrease in the star's brightness as the planet passed in front of its host star (Konacki et al., 2003). This became known as the "transit method," and to date, this method has detected more exoplanets than any other. The transit method only requires simple photometry, which can be done with significantly higher signal to noise than spectroscopy. Typically, transits are found using relative photometry; where the brightness of a star during transit is compared to the brightness of other stars in the field. This means that measurements can be accurate despite the presence of systematic errors. In a transit, the measured signal is the decrease in the brightness of the star relative to its normal brightness, so the measured value is called transit depth, and can be given by

$$D = \frac{R_p^2}{R_*^2}, \tag{2.4}$$

where D is the transit depth, R_p is the planet radius, and R_* is the star radius. Using the above example of a 1 $R_\oplus$ planet around a 0.17 $R_\odot$ star, the transit depth would be 0.0028, or $^3/_{1000^{\text{th}}}$ the brightness of the star, which can be measured fairly reliably. The most observable exoplanets are large planets around small stars. Small stars are less likely to drown out the signal of a planet, and large planets are likely to create larger signals. A large planet around a small star would have a large transit depth. Transit depth is usually reported in parts per million (ppm) instead of as a decimal, as it will for the remainder of this thesis.

Another useful method to detect exoplanets is through measuring the radial velocity of the host star. As an exoplanet orbits its host star, the star should move as well much more slowly than a planet. With the use of a spectrograph, the doppler shift of a host star can be measured. Usually a star may be moving at speeds so low, they're measures in centimeters per second, but it can still be measured reliably. By applying the laws of conservation of momentum, the relationship

$$m_* v_* = m_p v_p, \tag{2.5}$$

where m represents the mass, v represents the velocity, * represents the star and p represents the planet. The star mass is known from the star's temperature and size, and the planet's velocity can be deduced from Kepler's laws. This method can be useful for measuring the masses of large planets, but the radial velocity methods fails when the planetary mass is too small to produce a large stellar velocity. This method is much easier to implement, and is therefore how we detected the first exoplanets (Latham et al., 1989). The radial velocity method can often be used in conjunction with the transit method because transiting exoplanets will produce the strongest possible radial velocity measurements. For more complicated systems with multiple planets, the radial velocity method becomes more difficult, and other methods are more useful for measuring planetary mass.

Unfortunately, there are some major limitations to the transit method. The most scientifically interesting exoplanets are terrestrial exoplanets are approximately 1 $R_\oplus$, approximately 1 $m_\oplus$, and have approximately 1 $S_\oplus$. For large stars, smaller planet become impossible to detect as their transit

depth is too small. With even the best scopes, it can take years to measure terrestrial exoplanets around sun-like stars. The Earth-Sun system has a transit depth of 84ppm, which is orders of magnitude smaller than the average transit. A planet very similar to the Earth-Sun system called Kepler-452b has been found (Jenkins et al., 2015), but a recent study by Mullally et al. (2018) has argued that the system doesn't have strong enough signal to noise to be confirmed as an exoplanet.

Another major limitation is that only a small number of exoplanets orbit in an observable plane. If we assume that an exoplanet orbits in a random orientation relative to Earth, and we can only detect it if its orbital plane is within 3°, then $\sim 3\%$ of exoplanets can be detected from Earth. In reality, the actual cutoff of an "in plane" exoplanet is more complicated and depends on a number of other variables, but 3° is a good first-order estimate. Our ability to detect smaller transit depths will improve over time, but the inclination issue is an inherent limitation to the transit method. Only transiting exoplanets will be considered for the remainder of this thesis. The conclusions made with transiting exoplanets can be easily generalized for non-transiting exoplanets because there is nothing intrinsically different between transiting and non-transiting exoplanets.

For transiting exoplanets, there are a few coordinate conventions that must be described explicitly. The angular difference between the orbital plane and Earth is called the inclination, denoted here by θ. A visual example of inclination is given in Figure 2.1. The position of the exoplanet in its orbit is called the orbital phase. Conventionally, the phase where an exoplanet is perfectly behind its host star is set to 0° (an occultation, or sometimes a type-II transit), and the phase where an exoplanet is perfectly in the middle of a transit is set to 180° (also called a type-I transit). A visual explanation of phase is given in Figure 2.2. It doesn't matter which direction an exoplanet orbits, as long as the convention is consistent. In this paper, the orbital phase will be called ϕ and will be to the left for $0° \leq \phi \leq 180°$ and to the right for $180° \leq \phi \leq 360°$

A majority of exoplanets are found around small stars, mostly K-type and M-type stars, due to observational biases that favor detections in these systems. These stars are far redder than Sun-like stars, and emit far less light. This means that in order for a planet to receive similar irradiance to Earth, it must be much closer to its parent star. Exoplanets found in the habitable zones of

late-K and M-dwarf stars are likely to be tidally locked, meaning that they rotate synchronously with their parent star. The Moon is tidally locked to the Earth, which is why we always see the same face of the Moon, but it still rotates relative to the Sun. With exoplanets that are tidally locked relative to their parent stars, one half of the planet will receive constant sunlight, and the other side of the planet will receive none. In this situation, a new set of useful terminology can be used to describe constant points on the planet's surface. The point that is always facing the Sun is the substellar point. The point that is opposite to the substellar point is the antistellar point. The line that is equidistant from the substellar and antistellar point is called the terminator. The substellar point is equivalent to Earth at noon, where the sun is directly overhead; the antistellar point is equivalent to the Earth at midnight; and the terminator is equivalent to the Earth at sunset and sunrise.

Any point on a spherical object can be defined using two angles, and the most standard coordinate system is latitude (δ) and longitude (λ), where the equator is defined as $\delta = 0°$, the North Pole is $\delta = 90°$, and the South pole is $\delta = -90°$. Longitude ranges from 0 to 360, and on Earth, the "zero point" is completely arbitrary. In the case of tidally locked planets, we set the zero point to be conveniently aligned with the antistellar point, so the substellar point is at $(\lambda = 180°, \delta = 0°)$.

Of the exoplanets discovered, the TRAPPIST-1 system provides the most interesting case in the search for habitable exoplanets, and will therefore be a primary target for the upcoming JWST mission. Around the star TRAPPIST-1, there are 7 exoplanets, named alphabetically from b to h. They are all roughly $1 m_\oplus$ and $1 R_\oplus$. TRAPPIST-1 is a cool M-dwarf with a temperature of 2511 K, at a distance of 12 pc from Earth (Delrez et al., 2018). TRAPPIST-1 b has a solar irradiance of 3.8 $S_\oplus$, too hot for life. TRAPPIST-1 h has an irradiance of 0.13 $S_\oplus$, which is far too cold to support life. Since both ends extremes are present here, it's reasonable to hope that somewhere in the middle, one or two of the remaining 5 are similar enough to Earth to support life.

Using the work done by Turbet et al. (2018), it is reasonable to conclude that all the TRAPPIST-1 planets are tidally locked and have an eccentricity low enough to approximate it

as 0. With the known parameters of the TRAPPIST-1 system found by Gillon et al. (2017), the next logical step is to run climate models to more accurately estimate habitability.

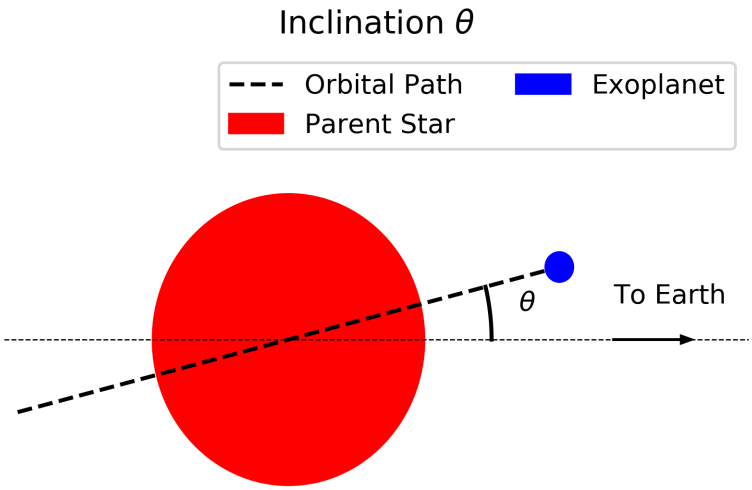

Figure 2.1: Simple depiction of inclination. Any possible exoplanet can be viewed from this angle, making inclination a universal tool for characterizing exoplanets. Typically, an exoplanet with an inclination of less than 3° can have a transit, although this isn't the most rigorous definition, and the actual value depends on planet size and star size. However, the closer to 90°, the better because that means longer transits and therefore better measurements.

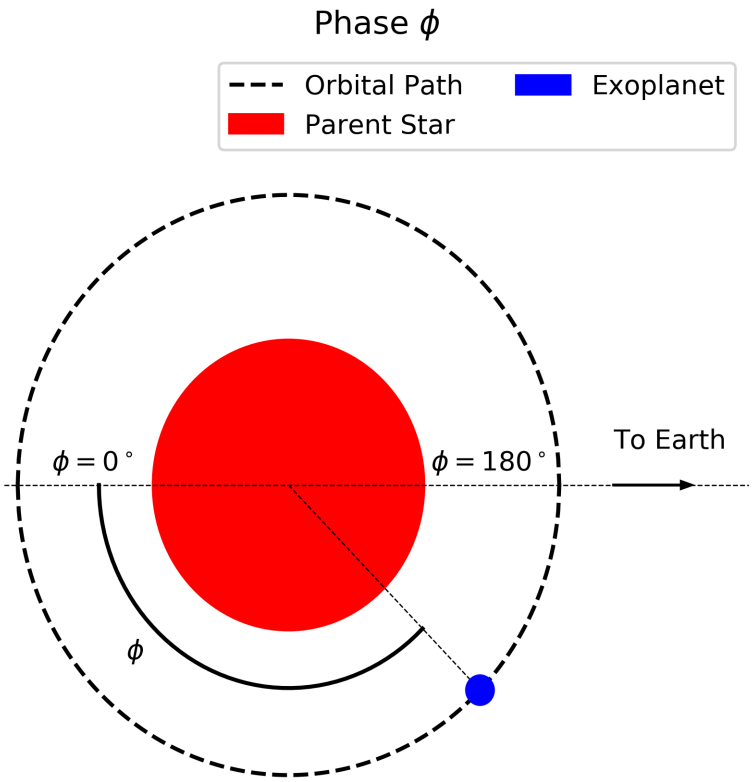

Figure 2.2: Simple depiction of phase. In this diagram viewing an exoplanet from above, phase first goes down, then up. The convention of phase can be defined relative to transits and occultations, and regardless of the direction of this convention, the math behind which latitudes face Earth remain constant. An occultation is set to $\phi = 0\,\mathrm{deg}$, and a transit is set to $\phi = 180\,\mathrm{deg}$.

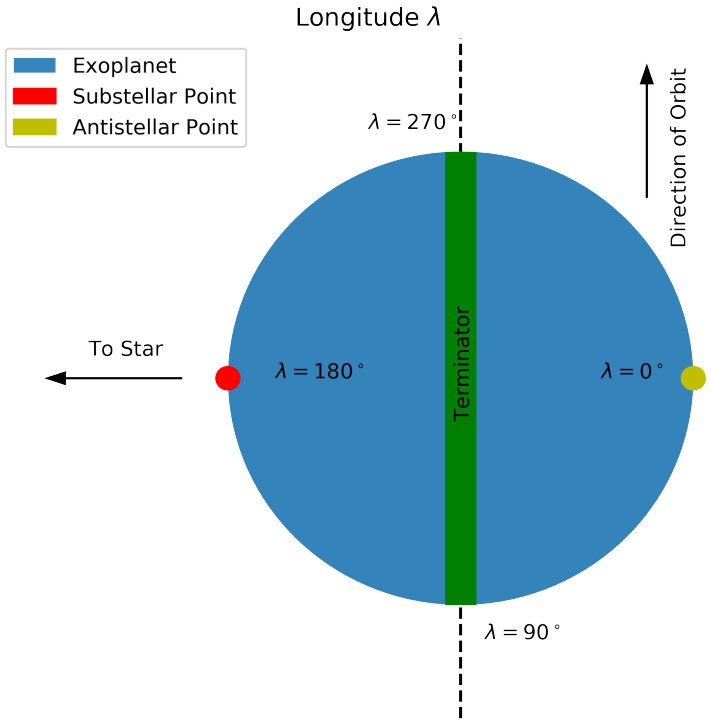

Figure 2.3: Simple depiction of longitude for a tidally locked planet. These longitudes are correct for any phase or inclination. Note that from Earth during a transit $\lambda = 0°$ when $\phi = 180°$, and the two variables move in opposite directions.

Chapter 3

Climate and Atmosphere Models

For this study, I used the 3D climate modeling simulations of Wolf (2017, 2018) as a starting point for analysis of spectral signals that may be detected with JWST and other telescopes. Therefore, it is important to review the results of the climate models in order to adequately understand any conclusions derived from them. Many of the conclusions discussed here will have significant impacts on Chapter 5 and 6.2. Transit spectra is sensitive to the atmospheric composition, and in order to characterize that sensitivity, many climate models with varying parameters must be tested. For thermal phase curves, clouds are particularly important because they determine the emissivity of the atmosphere. Climate models allow us to predict the distribution of clouds on the TRAPPIST-1 planets, giving us insight into what we would see from a thermal phase curve. Cloud distributions depend on the availability of water vapor, the temperature of the planet, and on the large scale atmospheric circulation, which itself depends on the strength of the Coriolis force, which is determined by the rotational rate of the exoplanet. Assuming that the TRAPPIST-1 exoplanets are tidally locked allows us to set their rotation rate to their orbital period, allowing us to precisely constrain the influence of the Coriolis force.

Climate models have proven to be a very useful tool to accurately predict behavior of an atmosphere. Climate models use fundamental physics like radiative transfer, convection, the Coriolis force, and other rules to predict the motion of air parcels iteratively through time. One popular climate model is the Community Atmosphere Model 4 (CAM4), provided by the National Center for Atmospheric Research (Neale et al., 2012). Using a modified version of CAM4, Wolf (2017,

2018) were able to apply climate models to the tidally locked exoplanets of the TRAPPIST-1 system including TRAPPIST-1 d, TRAPPIST-1 e, and TRAPPIST-1 f. All of the climate models for TRAPPIST-1 d entered a runaway greenhouse, even in models without CO_2. All of the models for TRAPPIST-1 f required multi-bar CO_2 atmospheres to maintain reasonable temperatures. TRAPPIST-1 e had numerous models which were habitable with low and moderate amounts of CO_2, making TRAPPIST-1 e is the most promising candidate of the system for supporting habitable conditions. Although other cases will be considered, this paper will focus primarily on TRAPPIST-1 e.

Climate models can be used to determine the impacts of a variety of atmospheric species. In these models, fixed amounts of CO_2 and N_2 were given, while H_2O is allowed to vary self-consistently by CAM4. CO_2 will always tend to warm an atmosphere because of the greenhouse effect. Only molecules with 3 or more atoms contribute to the greenhouse effect directly because they contain vibrational modes which can store energy levels that correspond to infrared wavelengths. Two-atom molecules like N_2 cannot contain vibrational modes, and thus cannot absorb or emit infrared light. However, adding N_2 to an atmospheric model will increase the pressure, which can impact the absorption of infrared light by CO_2. Unlike atomic emission features, which absorb and emit at discrete wavelengths, molecular emission features are broad, and although they peak at a fixed wavelength, they will emit or absorb light for a large range of wavelengths around the peak wavelength. Increasing the pressure of a greenhouse gas has the tendency to broaden this emission feature, and therefore increase its efficacy as a greenhouse gas. For this reason, adding N_2 to an atmosphere can also increase the atmosphere's average temperature. H_2O, like CO_2, is a greenhouse gas and exhibits pressure-broadening. More importantly, H_2O is not well mixed in an atmosphere, and may condense in the atmosphere as liquid clouds, ice clouds, or vapor, as well as condense on the surface as ice, snow, or water. The primary advantage of running a 3D climate model is to allow for self-consistent calculations of water in its various phase, as distributed across a planet by general circulation.

Recently, Wolf has included CH_4, which is a stronger greenhouse gas than CO_2 or H_2O.

Shown in Table 3.1 is a list of all the TRAPPIST-1 e models used in this study. Many of the models for TRAPPIST-1 e have global mean temperatures that appear too low or too high to support life. The Earth's mean atmospheric temperature is $\sim 287\,\mathrm{K}$ (Wang et al., 2005), and some of the models produce similar temperatures. From this list, the most interesting models are the $1\,\mathrm{bar}$ N_2, $0.2\,\mathrm{bar}$ CO_2, and $1\,\mathrm{bar}$ N_2, $0.4\,\mathrm{bar}$ CO_2 because they have a global mean temperature closest to that of modern day Earth, although some others also stand out as strong candidates for habitability.

Despite what Table 3.1 and Figure 3.1 suggest, habitability is more complicated to define. Most of the details about habitability are questions of biology. Many finer details about how life would operate cannot be inferred from these models. All of these models use a global ocean but ignore ocean currents, which is a major method of heat transport on Earth. However, a recent study by Yang et al. (2019) that used exoplanet GCMs that considered ocean currents concluded that ocean heat transport is important primarily for cold tidally locked planets. Warm tidally locked planets with mean temperatures above 280K already have efficient atmospherics heat transport. None of the models include land masses, which would change both ocean currents and atmospheric currents. Many significant atmospheric species like O_2, O_3, N_2O, and others are not included, despite their obvious significance in Earth's atmosphere. CO_2 abundance is set as a model parameter, but in reality, its abundance would be driven by geologic processes over timescales much longer than where CAM4 would be useful. Some geologic models of exoplanets have found that negative feedbacks between CO_2 and H_2O will tend to cause the partial pressure of CO_2 to converge to a habitable value with liquid water (Kite & Ford, 2018).

In addition to climate models, equations used to predict Earth's atmosphere can help us describe the TRAPPIST-1 system. Anthropogenic climate change on Earth was predicted by Dr. Svante Arrhenius, who created an effective equation to predict the warming of an atmosphere, given

N_2 bar	CO_2 bar	CH_4 bar	H_2 bar	Surface Temperature K
0	0.25	0	0	237.7
0	0.5	0	0	268.0
0	1	0	0	303.0
0	2	0	0	333.2
0.9	0	0	0.1	229.2
1	0	0	0	217.4
1	0.0004	0	0	234.2
1	0.0004	1.7×10^{-6}	0	236.1
1	0.01	0	0	248.1
1	0.1	0	0	270.2
1	0.2	0	0	281.5
1	0.4	0	0	301.0
1	1	0	0	330.2
1.5	0.1	0	0	280.9
1.5	0.2	0	0	294.9
2	0.1	0	0	286.7
2	0.2	0	0	306.1
4	0.1	0	0	319.0
4	0.2	0	0	332.2
10	0.2	0	0	358.4

Table 3.1: TRAPPIST-1 e Models and Species Abundances. Each row represents a single climate model of TRAPPIST-1 e, with each column showing the amount of a given species in that model. The surface temperatures are an average of the entire planet surface.

an increase in CO_2. Arrhenius' rule is given as

$$T = \alpha \ln\left(\frac{C}{\mathrm{C_0}}\right) + \mathrm{T_0}, \tag{3.1}$$

where C is the current amount of CO_2 in the atmosphere, $\mathrm{C_0}$ is the former amount of CO_2 in the atmosphere at a given time, and $\mathrm{T_0}$ is the global atmospheric temperature at that time, α is a constant that depends on a number of variables not considered in this model. For TRAPPIST-1 e, this equation can be used to interpolate between specific climate models. In Figure 3.1, this equation produces a reliable line of best fit. A similar fit can be made for increasing N_2, and is shown in Figure 3.2.

For the purposes of transits, the terminator is the only significant section of the atmosphere, but for thermal phase curves, spatial resolution is a necessity, largely due to the presence of a substellar cloud (Kopparapu et al., 2017). CAM4 models the atmosphere using a discrete number of points, making a 3D array of coordinates where there are 72 longitudinal bins, 46 latitudinal bins, and 40 vertical bins. Each attribute of a model (like temperature, cloud amount, etc.) all have their own data cubes. In order to display the data, it must be reduced from a 3D set. A useful method of displaying data like cloud abundance is using a column density. Each vertical layer of the atmosphere has a different cloud abundance, but we're mostly concerned with he total cloud abundance, which would be the sum of all the different layers. This more closely represents what the clouds would look like to a distant observer. Figures 3.3 and 3.5 are both column densities of liquid cloud abundance and precipitation.

A major influence on the structure of clouds in an atmosphere is the Coriolis force. The acceleration due to the Coriolis force is given as $\mathbf{a_C} = 2\mathbf{v} \times \mathbf{\Omega}$, where $\mathbf{v}$ is the velocity of a particle and $\mathbf{\Omega}$ is the rotational frequency of the planet. Earth has a rotational frequency of $^{2\pi}/_{24\,\mathrm{h}}$, so the Coriolis force plays a major role in atmospheric physics. TRAPPIST-1 e has no rotation relative to the Sun, but because its year is only 6 days (Gillon et al., 2017), it will have an angular frequency of $^{2\pi}/_{6\,\mathrm{d}}$, which is significantly less than Earth's, but still strong enough to drive significant zonal

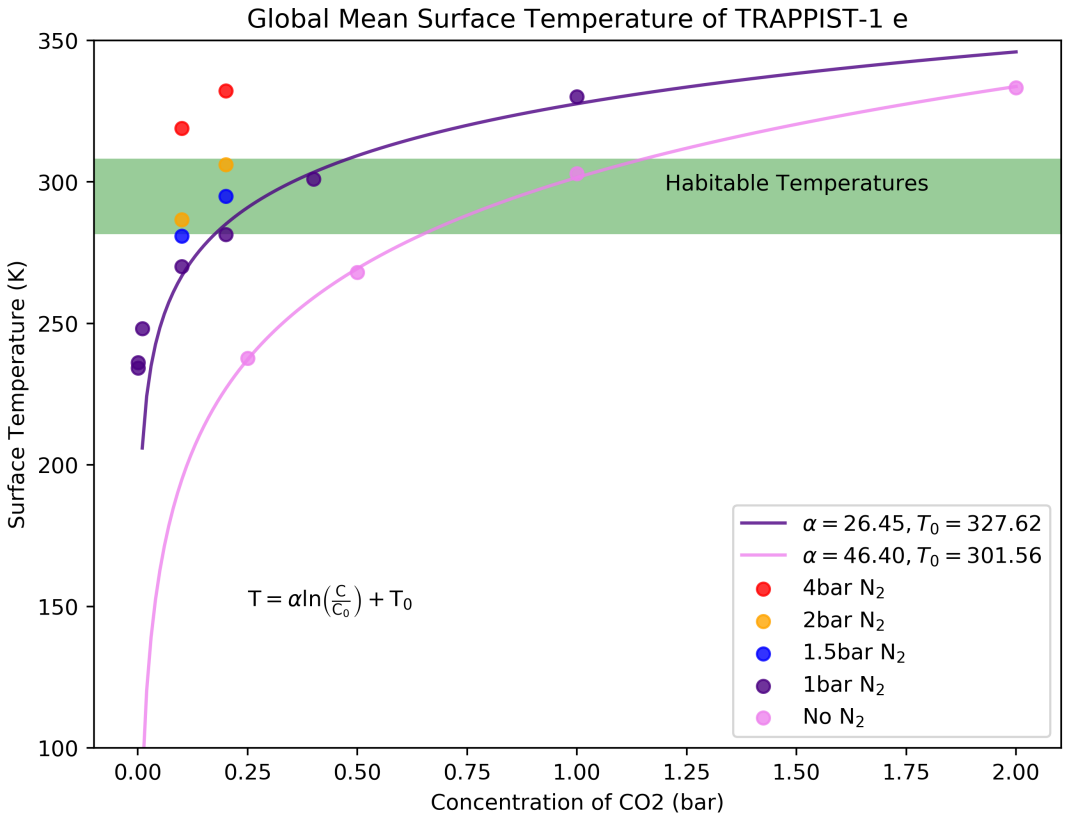

Figure 3.1: Globalmean surface temperature versus CO_2 partial pressure. Most of the models in Table 3.1 are shown here to more accurately demonstrate the relationship between CO_2 and warming. Both CO_2 and N_2 can contribute significantly to the warming of the planet, but they do so differently because N_2 is not a greenhouse gas. In this diagram, the "habitable zone" is between 275K and 315K, following the definition by Wolf (2017).

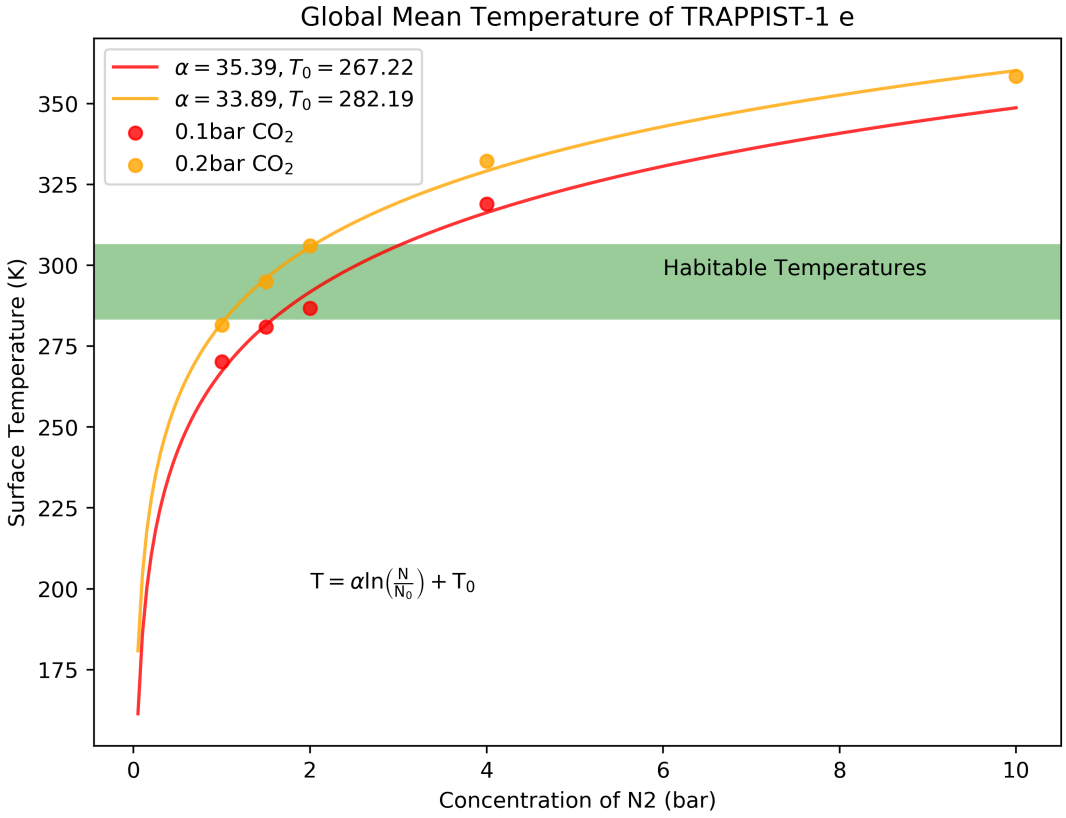

Figure 3.2: Globalmean surface temperature versus N_2 partial pressure. Similarly to Figure 3.1, logarithmic best fit lines match the data well, although the fit is noticably better for CO_2 than N_2.

circulation. The effects of TRAPPIST-1 e's Coriolis force can be clearly seen in Figure 3.3. The substellar cloud is fairly small, and is concentrated to the east, while the western side has little to no clouds.

Kopparapu et al. (2017) has run models on other synchronously rotating exoplanets, including some idealized exoplanets with set parameters such as solar irradiance and orbital period. These models can be put into two categories, fast rotators and slow rotators. An extended orbital period means that the Coriolis force is much weaker, which produces a different shape for its substellar cloud. The substellar hemisphere is covered by clouds, and the substellar cloud is fairly symmetric from the east to west and north to south. According to Haqq-Misra et al. (2018), fast rotators have a period of less than 5 days, slow rotators have a period of greater than 20 days, and the region in between is called the Rhines rotation regime. TRAPPIST-1 e, on the boundary between the two, exhibits characteristics of both. For the purposes of this investigation, the most important atmospheric feature is a contained and persistent substellar cloud, shown in Figure 3.3. Slow rotators (like the 44 day one shown in Figure 3.4 have large substellar clouds that are highly symmetric and cover most of the planet's day side.

In addition to surface features, one of the most useful tools to describe a planetary atmosphere is its profile. During an exoplanet transit, light will pass through the atmosphere, and the lower atmosphere will be too opaque, and little light will make it through, but the upper atmosphere will be much less dense, allowing more light through. This means that atmospheric features that are close to the planet's surface would be much harder to detect compared to upper atmosphere features. Figure 3.6 shows that a majority of the clouds are concentrated in the lower atmosphere, meaning that H_2O will be harder to see in an exoplanet transit than CO_2 which is well mixed at all levels of the atmosphere. From Figure 3.6, a thermal inversion close to the surface can also be seen, meaning that the temperature goes up with height for a brief period. This has the effect of stabilizing the atmosphere and on Earth, can cause pollution to be trapped near the surface (Fortelli et al., 2016). In this plot, the effective temperature is given, which is what the temperature of the

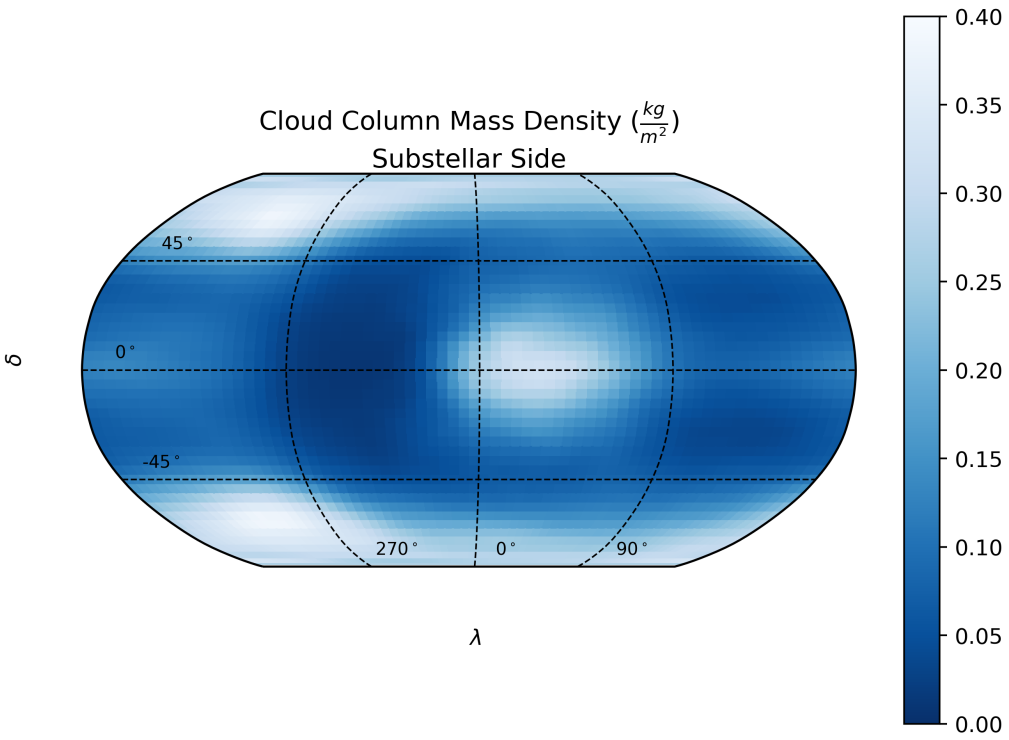

Figure 3.3: Cloud Column Density of TRAPPIST-1 e with 1 bar N_2 0.4 bar CO_2. In this image, white represents very dense clouds, and blue represents few to no clouds. For the substellar point, there are strong clouds, particularly on the eastern side. Surprisingly, right next to the substellar point is also the region with the least amount of clouds. This is due to the planet's rotation, which causes a Coriolis force that produces asymetric substellar clouds.

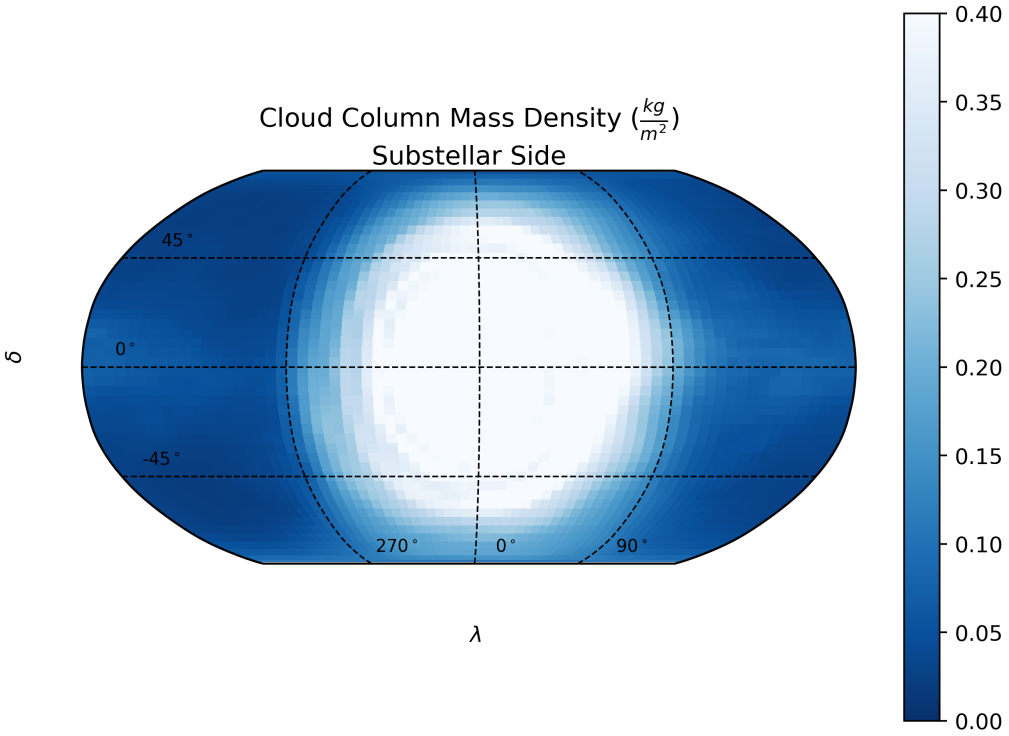

Figure 3.4: Cloud Column density of a slow rotator. The planet used here is a slow rotator with an orbital period of 44 days. In this case, it received significantly more solar energy from TRAPPIST-1 e, which will cause it to be extremely warm and therefore have much stronger clouds than TRAPPIST-1 e. The absolute scaling of the cloud amount is less important than the shape of the clouds. Here, the clouds are extremely symmetrical and large. This is a dramatic difference from the behavior of the TRAPPIST-1 e model in Figure 3.3.

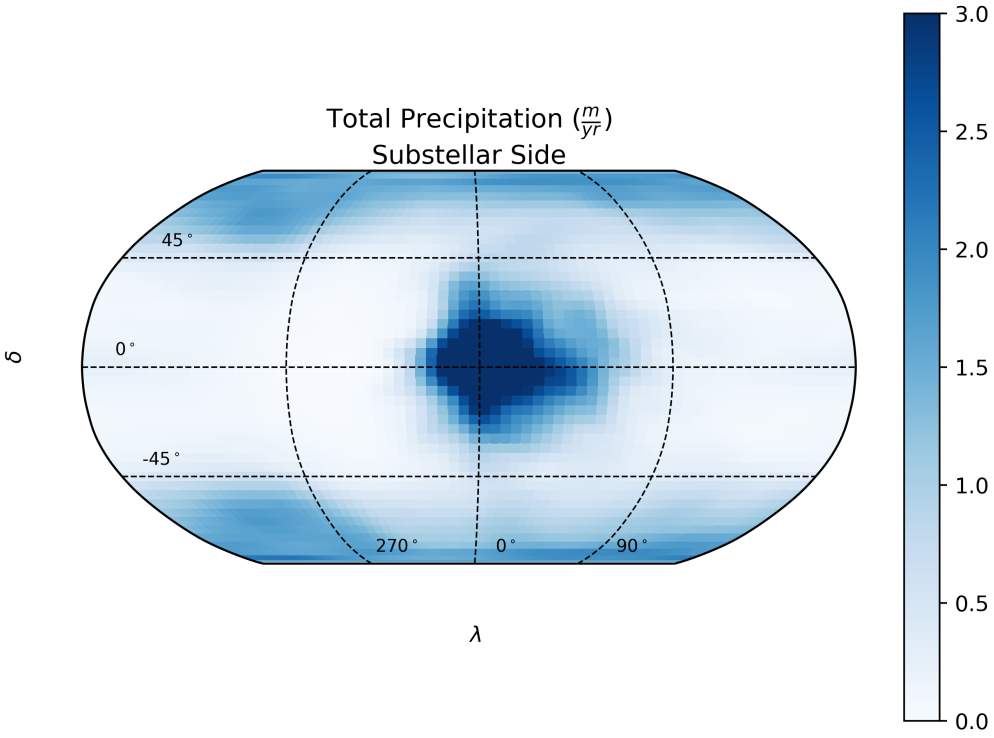

Figure 3.5: Precipitation of TRAPPIST-1 e with 1 bar N_2 0.4 bar CO_2. In this image, blue represents high amounts of precipitation and white represents little to no precipitation. From Figure 3.3, we can conclude there is a persistent substellar cloud, but in order to determine if there's actually rain reaching the surface, one must also check its precipitation since the presence of clouds doesn't always mean there must be rain. There does appear to be very localized substellar rain indicated by the blue dot, but the rest of the planet only has marginal amounts of rain in comparison.

planet's surface would be if it had no atmosphere, and is given by the equation

$$T_e = \sqrt[4]{\frac{\mathrm{S}(1-\alpha)}{4\sigma}}, \tag{3.2}$$

where T_e is the equilibrium temperature, S is the solar irradiance, α is the albedo, and σ is the Stefan-Boltzmann constant. The equilibrium temperature is a useful benchmark for a planetary atmosphere as it represents a lower limit on the planet's surface temperature.

While these models illustrate many characteristics of the TRAPPIST-1 e atmosphere, there are a number of noteworthy assumptions that limit our predictive capabilities. These models do not include O_2, which is a vital element for living organisms. Adding O_2 would dramatically complicate the models because it would require a prognostic chemistry calculation, which would imply the addition of O_3 as well, a greenhouse gas and the primary species in the stratosphere. These TRAPPIST-1 e models also do not include a stratosphere, which would be a second thermal inversion higher up in the atmosphere. These models are long term models run over 40 years, and they only have enough resolution to determine general features. Unlike a weather forecast model; these models cannot accurately predict small weather features in the TRAPPIST-1 e atmosphere, the models are only useful for general, long-term trends. These climate models do not include any trace atmospheric species, most notably N_2O, but there are many more species that could be detected during a transit from a telescope.

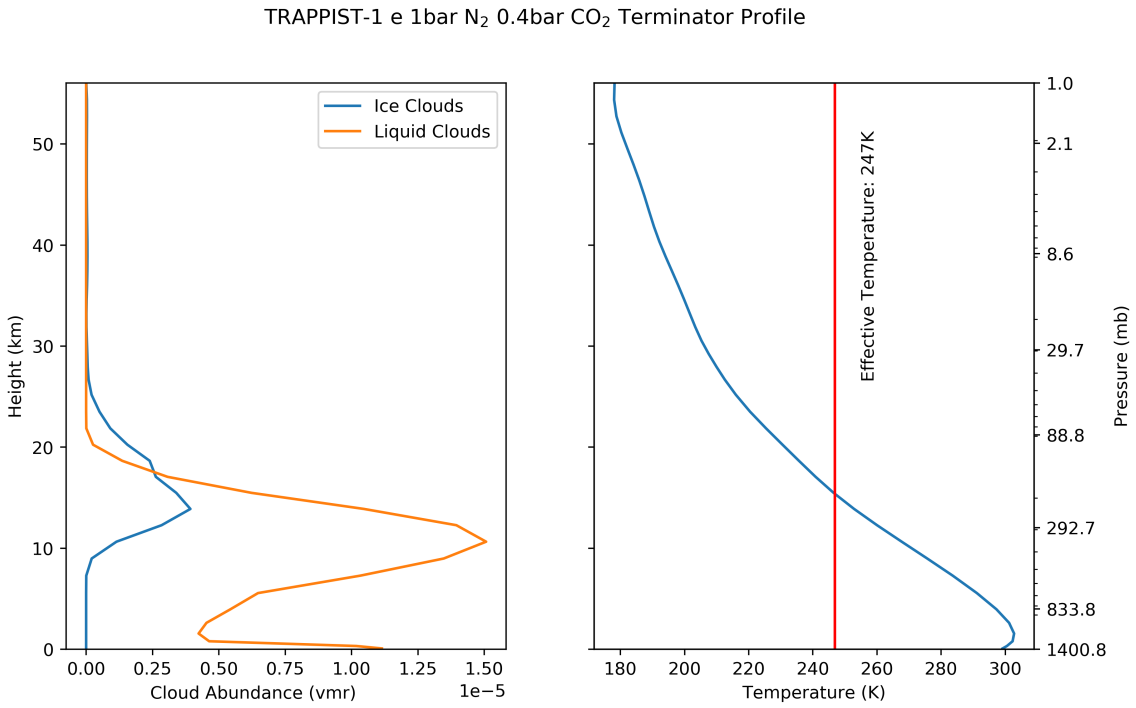

Figure 3.6: Profile of TRAPPIST-1 e with 1 bar N_2 0.4 bar CO_2. The left plot shows the distribution of ice and liquid clouds in the atmosphere. Ice clouds are more abundant higher up than liquid clouds. There are also more liquid clouds than ice clouds overall, as represented by the surface area under them. The right plot is a diagram of temperature across altitude. Close to the surface, there is a temperature inversion, stabilizing the surface air. Above that, the temperature decreases with height continuously.

Chapter 4

Methods

The James Webb Space Telescope is set to launch some time in 2021, with a cost of over $8.7 billion in the first five years after launch. We need to be able to accurately predict how it will operate before it launches in order to effectively allocate observation time. The Planetary Spectrum Generator (PSG) created by Villanueva et al. (2018), was designed specifically with this in mind, and can simulate a variety of planetary observations using a variety of telescopes. The PSG's most important feature is its line-by-line radiative transfer model (PUMAS), which depends strongly on the given atmosphere profile. The climate models discussed in chapter 3 provide a useful input to the PSG, but because the climate models are complex, they must first be adapted into formats supported by the PSG. The bulk of the work for this thesis was to create a data pipeline to make climate models compatible with the PSG. In this chapter we will discuss the techniques used to convert the models from Wolf (2017, 2018) into inputs for the PSG and how the PSG uses those inputs to produce spectra.

Climate models have many outputs. Attributes such as temperature, species abundance, pressure, and others are stored in latitude by longitude by altitude arrays. Other parameters such as surface temperature, albedo, and surface pressure are stored in latitude by longitude arrays. Other parameters have only one planet-wide value like gravity and orbital period. The output of climate models are a complex file type that stores all these values, but only a few of them are relevant for the PSG. Additionally, some values are not included in the climate model such as the distance between the star and the observer, the orbital inclination, and others. These parameters

are astrophysically important, and are therefore needed by the PSG, but are not provided by the climate model because they are not atmospherically important, so they must be found elsewhere.

Additional parameters that were not given by the climate model were found using NASA's exoplanet archive. The parameters used from the exoplanet archive were name, mass, radius, diameter, semi-major axis, inclination, transit depth, insolation, star radius, star velocity, star effective temperature, star distance, star magnitude, star metallicity, and star logarithmic surface gravity, and are specific to TRAPPIST-1 e.

The PSG only uses an atmospheric profile, so the 3D climate model data had to be reduced to a 1D atmospheric profile. How this should be done depends on the observational conditions. For an exoplanet transit, the significant part of the atmosphere is the terminator profile because that is where light from the star will pass through the atmosphere and towards the observer. For all other phases, the most significant part of the atmosphere is the Earth facing side.

For a transit the phase is 180°, which means the left hand side has a phase of 270° and the right hand side has a phase of 90°. For the models in Wolf (2018), these phases correspond to exactly a single grid cell, but in order to generalize the procedure, the average of all cells that fit the criteria of $\lambda = 270° \pm 5°$ **or** $\lambda = 90° \pm 5°$ is used. This method would work even if there was no longitude corresponding exactly to $\lambda = 270°$ **or** $\lambda = 90°$.

For a transit, all longitudes and latitudes are weighted equally because the grid cells are spaced evenly across latitudes. In order to compute a transit profile, the points are averaged with equal weighting according to the equation

$$x_i(\phi) = \frac{\int_{85^\circ and 265^\circ}^{95^\circ and 275^\circ} \int_{-90^\circ}^{90^\circ} x_{i,\delta,\lambda} \, \mathrm{d}\delta \, \mathrm{d}\lambda}{\int_{85^\circ and 265^\circ}^{95^\circ and 275^\circ} \int_{-90^\circ}^{90^\circ} \mathrm{d}\delta \, \mathrm{d}\lambda}, \tag{4.1}$$

where x is a parameter at a grid cell of height i, latitude δ, and longitude λ. Latitude and longitude are averaged, but the heights are not, so Equation 4.1 would reduce a 3D climate model to a 1 dimensional profile for each parameter x. The parameter x can be used to represent temperature, pressure, or volume mixing ratio of any of the tracked species.

For the non-transits, many of the variables that were fixed in the transit case are no longer constant. To create a non-transiting atmosphere profile, the longitude (implicitly as a function of phase) is now a variable. In transits, all grid point are equally significant to the atmosphere profile, but for a non-transiting profile, some points are more significant than others. Inherent to a latitude-longitude grid is the convergence of points near the poles. The result is that each grid cell occupies less area near the poles, and should therefore be weighted less in the average by a factor of $\cos(\delta)$. In addition, the Earth facing side contributes more to the emission towards Earth than the limbs. The result of this is a second factor of $\cos(\delta)$ to account for the latitudinal component and a factor of $\cos(\lambda + \phi)$ to account for the longitudinal component. The resulting value is a disk average given by the equation

$$\mathrm{x}_i\left(\phi\right) = \frac{\displaystyle\int_{-\phi-90^\circ}^{-\phi+90^\circ}\int_{-90^\circ}^{90^\circ} \cos^2(\delta)\cos(\lambda+\phi)\mathrm{x}_{i,\delta,\lambda}(\phi)\ \mathrm{d}\delta\,\mathrm{d}\lambda}{\displaystyle\int_{0^\circ}^{360^\circ}\int_{-90^\circ}^{90^\circ} \cos^2(\delta)\cos(\lambda+\phi)\ \mathrm{d}\delta\,\mathrm{d}\lambda}, \tag{4.2}$$

which is the same as Equation 4.1, except for the addition of a weighting in the cosine of λ and δ, and a dependence on ϕ. Physically, this equation can be described as taking a 3D sphere of the planet and simplifying it to a 2D projection as seen by the observer, then averaging the observed value (Cowan & Agol, 2008; Koll & Abbot, 2015). This method means that any atmospheric parameter x that varies with respect to ϕ should change relative to the observer. The cosine squared for latitude indicates that there is a strong preference for latitude, and atmospheric features that are significantly north or south of the equator should only weakly contribute to the disk averaged value.

This disk weighted average explicitly shows the weighting function used, but implicitly in the integrals, there is also a mask, where only half of the planet is used in the calculation at any given time. This is because only half of the planet is facing Earth, and the other half therefore shouldn't contribute to the average. If the limits were to include the anti-Earth facing side, it would include negative values due to the cosine term, which would be nonsensical. In Figure 4.1, these two behaviors are shown side by side.

For transits, a different masking scheme is used, and no weighting scheme is used. A similar

diagram to Figure 4.1 is given for the transit case in Figure 4.2.

The whole purpose of averaging these values is that the 3D climate model can be reduced to an atmosphere profile that can be put into the PSG. The parameters used from the climate model profile were height, pressure, temperature, and the volume mixing ratios of N_2, CO_2, CH_4, H_2O, liquid clouds, ice clouds, liquid cloud size, ice cloud size. Additionally, surface pressure, surface temperature, surface albedo, and dry molecular weight were used, but they do not vary with height, so they are not part of the profile, although they are still taken by the PSG as a separate parameter.

In an exoplanet transit, light passes through the atmosphere and is collected by a telescope. A majority of an exoplanet's atmosphere is far too thick for light to enter one side and exit the other. As light passes through any medium that could absorb it, it should be extinguished according to Beer's Law

$$\frac{I}{\mathrm{I_0}} = \exp(-n\sigma L), \tag{4.3}$$

where I is the intensity of the light as seen by the observer, $\mathrm{I_0}$ is the intensity of the light at the source, n is the particle number density, σ is the cross-sectional area of the particles, and L is the length of the path that light travels. In an exoplanet transit at low altitudes, n is far too large, so $I/\mathrm{I_0}$ is too small to be detected. While σ won't vary much across an atmosphere, n and L will decrease as a function of height. n will decrease exponentially as given by the equation

$$\frac{n}{\mathrm{n_0}} = \exp\left(-\frac{z}{\mathrm{H}}\right) \tag{4.4}$$

$$H = \frac{\mathrm{k_B}T}{\mathrm{mg}}, \tag{4.5}$$

where z is the height, n is the volume density, $\mathrm{k_B}$ is the Boltzmann constant, T is the atmospheric temperature, m is the average molecular weight, and g is the gravitational force. This means the upper atmosphere will be much less dense than the lower atmosphere. The CAM4 climate models only have grid points down to 1 mbar. Pressures below 1 mbar are not considered as they are not significant for atmospheric dynamics. However, for transit spectra, 1 mbar is still relatively

opaque, and n must be decreased even more for significant amounts of light to pass through the atmosphere. To amend the atmosphere models for the purposes of transit spectra, additional layers must be added to the atmosphere, and these layers must also have pressure drop off exponentially. While temperature decreases with height for most of the atmosphere, this effect is ignored, and all the added layers have a constant temperature given by the top layer of the climate model. Additionally, the ratios of all atmospheric species are kept the same as the top layer of the climate model.

For the purposes of the PSG, only a few layers were added because the PUMAS radiative transfer model includes a very accurate sub-layering scheme. For all simulations used in this project, 7 layers were added, and the top layer was at a pressure of 10×10^{-6} mbar. Pressures this low are well beyond the necessary range and guarantee that the PSG will have atmospheric inputs capable of simulating an exoplanet transit.

The PSG can produce a variety of outputs, the most fundamental of which are $\mathrm{W\,m^{-2}\,sr^{-1}\,\mu m^{-1}}$ and ADU, which represent what a telescope would actually see. The PSG can also return an already reduced output that simply shows the transit depth. This reduced method can be derived from either raw method, but is more convenient for analysis, and is therefore the most commonly used. The PSG can produce a spectra, as well as a breakdown of its components by sources, although it's worth noting that none of those components can actually be observed in an exoplanetary system. In an actual exoplanet observation, only the raw total signal can be observed.

The results from the PSG separate the noise from the signal, although that's not how it would actually be observed. Signals without noise allow us to make predictions about observations, and noise can be used later to determine how long it would take to make conclusions about those observations. There are other noise simulators for JWST that rival that of the PSG, and often could use the PSG's spectra as an input. For this reason, the PSG only needs to be run once to get results on the signal, and the exposure time doesn't impact those results. Exposure time would only affect the signal-to-noise ratio.

For transits, the PSG needs to be run only once using the terminator mean profile. For

thermal phase curves, the thermal emitted flux must be computed at each point of the planet's orbit, so the PSG must be run multiple times to compute a thermal phase curve. Thermal phase curves should vary continuously, and so one might assume that they could compute thermal phase curves with arbitrary resolution. However, this isn't possible using 3D climate models because the averaged atmosphere profile won't change unless ϕ varies by more than 5° because that is the longitudinal resolution of the climate models. In Figure 4.1, the individual grid cells of the climate model can be seen by eye. The grid cell size defines the limiting temporal resolution of a thermal phase curve. This means that in order to compute thermal phase curves with higher resolution than 5°, it would require higher resolution climate models. However, the point is moot, TRAPPIST-1 e has an orbital period of 6.01 d (Gillon et al., 2017), and therefore orbits at a rate of $\sim 2.5\,^{\circ}\,\mathrm{h}^{-1}$. In an actual observation of a thermal phase curve, it's reasonable to be observing for multiple hours, so a climate model with 72 longitudinal bins will have similar or greater resolution in ϕ than the maximum possible resolution from observations in ideal conditions.

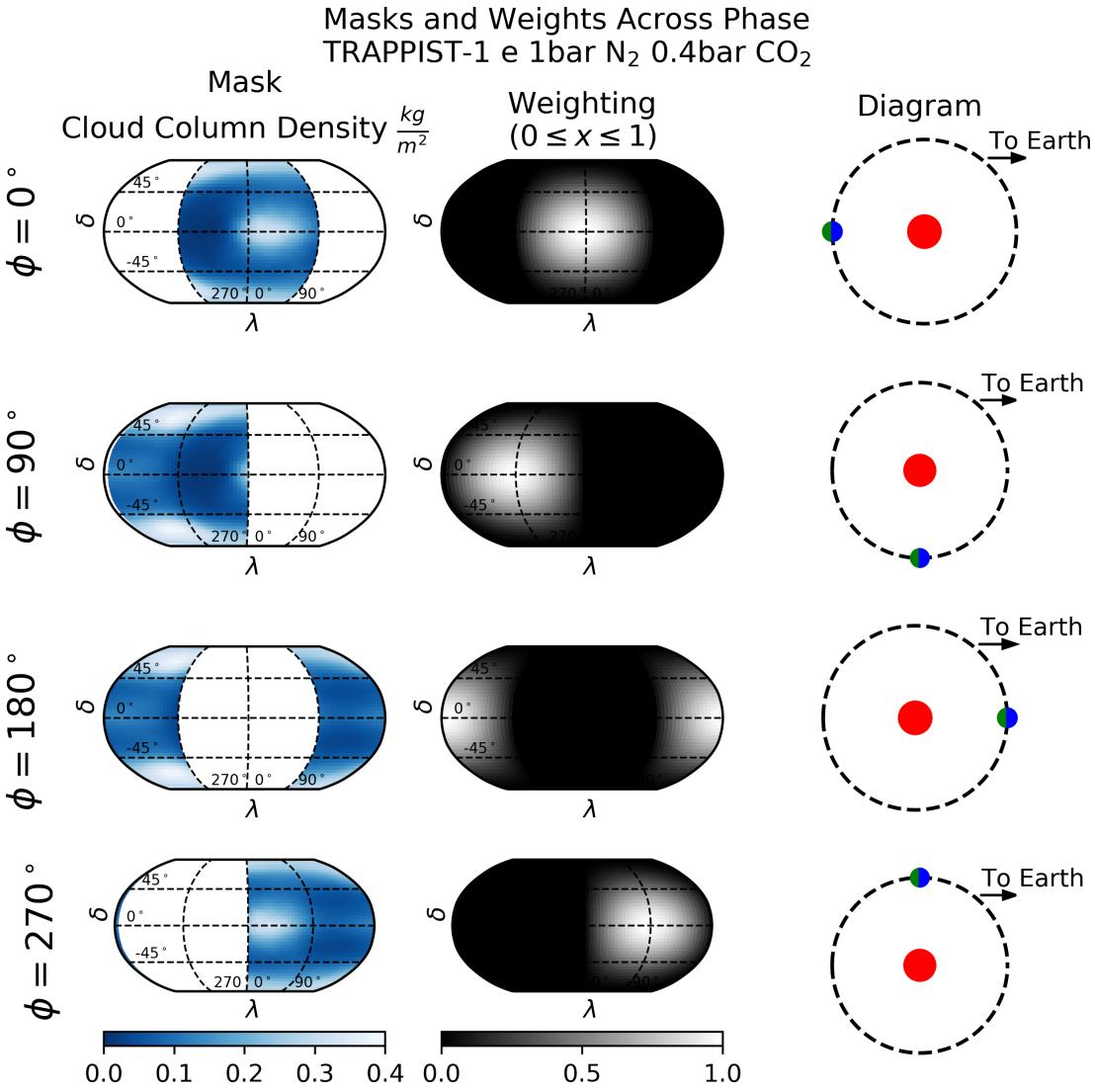

Figure 4.1: Surface masks and weights across phase. As a planet rotates through *phi*, the Earth facing side of the planet will change. The climate model used in the mask diagram is the TRAPPIST-1 e 1 bar N_2 0.4 bar CO_2 case. At different points through the year, the substellar cloud will move in and out of view. Parameters like emissivity should decrease as the cloud is in view and increase when the western side without clouds are in view.

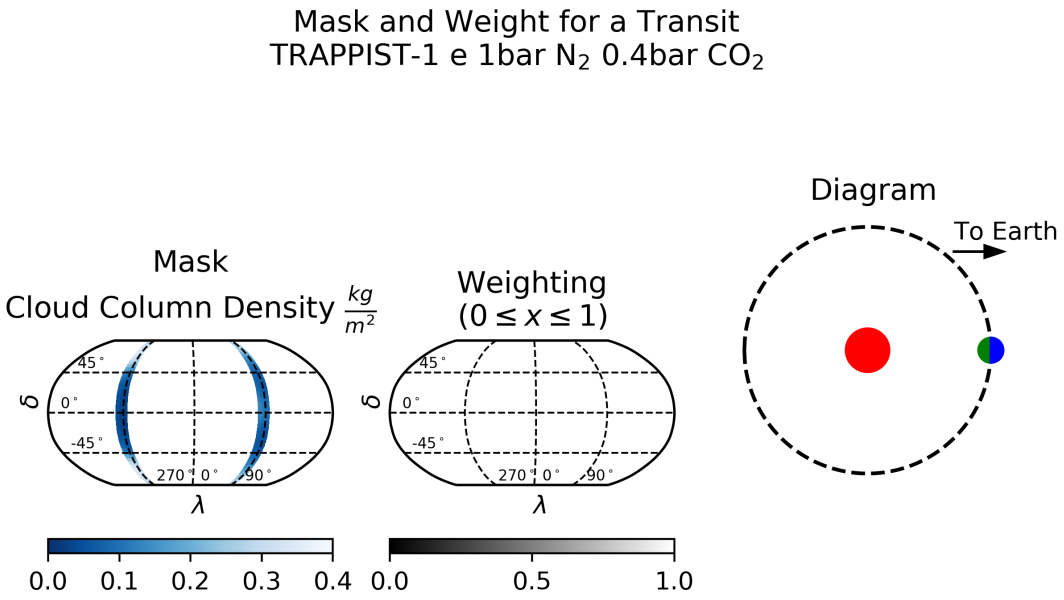

Figure 4.2: Surface masks and weights for transits. For the transiting case, a weighting function is unnecessary, but it is included for consistency with Figure 4.1. The more significant detail is that the masking scheme is discontinuous with the disk averaged values over the remainder of the exoplanet's year.

Chapter 5

Transit Spectra

Exoplanet transits have become the most consistent means of detecting exoplanets, and exoplanet transit spectra has become the most common method of analyzing an exoplanet's atmosphere. Before the launch of JWST, quality spectra have been difficult to produce and is often limited to visible wavelengths. The most observable planets for exoplanet spectra are hot Jupiters because they will have a large atmosphere and large transit depths, and even in those cases, Earth-based telescopes have had low signal to noise and spectral resolution. Recent observational work including von Essen et al. (2018) and Ducrot et al. (2018) have shown promising results, but have also shown that before the launch of JWST, models and theory are far ahead of observations. Using the PSG, we will be able to see spectra that is at James Webb's maximum resolution without noise, which will enable us to explore spectra and analyze it in ways that will not be observationally possible even after JWST launches.

The PSG can return spectra for a variety of JWST instruments, including MIRI-MRS (mid infrared, medium resolution), MIRI-LRS (mid infrared, low resolution), NIRSpec 2700 (near infrared, medium resolution), and NIRSpec 1000 (near infrared, low resolution). The range of wavelengths that can be measured range from 1 µm to 28 µm. The shorter wavelengths are usually referred to as the near infrared, which can sometimes be viewed from ground based telescopes. The longer wavelengths are in the mid-infrared, and are sometimes called the thermal infrared because while the near infrared features mostly absorption and emission features of molecules, the longer wavelengths are dominated by blackbody radiation of cool objects.

Transit spectroscopy's primary strength is its ability to detect atmospheric species, and the shorter wavelengths will produce the most significant results. In Chapter 6, I will show that beyond 17 µm, the thermal emission of an exoplanet dominates over absorption features.

In a noiseless spectra, it is often convenient to show as much information as possible, which can be done by combining the NIRSpec and MIRI instruments to produce a single spectra. This result for 1 bar CO_2 and 0.4 bar N_2 is shown in Figure 5.1. Over a small range around 5 µm, the two overlap. The axis are scaled logarithmically to emphasize the shorter wavelengths as they will generally have better signal to noise. The signals are reported in parts per million, relative to the star. A series of features can be easily identified, the most obvious of which is the 15 µm spike caused by CO_2. Some of the features are due to H_2O, but few to no features are due to N_2 because it does not absorb in the infrared. However, collisional processes involving N_2 can cause absorption (Afrin Badhan et al., 2019), but this is generally overwhelmed by CO_2 and H_2O absorption features.

For exoplanet transit spectra, the vertical axis is called transit depth, but it is slightly different than the transit depth D discussed previously. It is a spectral transit depth, $D(\lambda)$. Instead of describing the size of the planet and atmosphere, it describes the size of the planet and atmosphere at a specific wavelength. $D(\lambda)$ based on the atmospheric species that absorb at that wavelength. The 15 µm spike would indicate that the atmosphere is effectively larger at that wavelength due to CO_2, and therefore less of TRAPPIST-1's light will make it to the telescope. In effect, $D(\lambda)$ indicates absorption, and the cause of this dip will indicate composition. In general, these spectral lines would be compared to a list of spectral lines measured in a lab. We can skip this step with the PSG and by modifying the input atmosphere profile. Instead of sending the standard profile to the PSG, modified atmosphere profiles can be created, which can then be compared to the standard outputs. For example, to determine which features are due to H_2O, the PSG pipeline can be rerun, but with the H_2O abundance artificially set to zero (including the liquid and ice clouds). The outputs from the PSG can then be compared, and the difference between the two spectra is the effective contribution of H_2O. This procedure can be done for CO_2, H_2O, and N_2, all of which are shown together in Figure 5.2. Additionally, this plot demonstrates the validity of

adding additional layers to the atmospheric profile as was discussed in Chapter 3, one of the most significant assumptions made in the creation of this spectra. In this figure, the spectra without the additional layers has an artificial ceiling around 15 µm because the PSG found the atmosphere to be completely opaque in those wavelengths. Adding the additional layers shows a stronger signal because the atmosphere continues to be opaque at pressures much below 1 mbar.

From Figure 5.2, it is clear that the wavelengths between 12 µm and 18 µm are almost completely dominated by CO_2, but it is surrounded on all sides by various H_2O features, the strongest of which is at 6 µm. It is in diagrams like this where the absence of other atmospheric species is most noticeable. O_3 would produce a large spike at 9 µm, as well as other areas. The addition of many species would make the spectra more complex and more realistic.

Several of these larger features would be more easily detectable, even when MIRI is used in a low-resolution configuration. The features stand out primarily because they are wide as well as deep, and both are essential for strong signal to noise. The question then becomes "how strong is this signal and can it be used to detect H_2O from Earth?" Before we can consider analyzing signal to noise ratios, we must first create a method of measuring these variances that we can see in Figure 5.2.

For an example, we will focus on measuring the CO_2 in the MIRI spectra. Using the values from Figure 5.2, we can define a subset of the total wavelength range of MIRI where CO_2 is significant. We can define this region using the condition $D(\lambda) - D(\lambda)_{\text{No } CO_2} \geq 5\,\text{ppm}$. Any wavelength that matches this condition will be considered a significant wavelength for CO_2, and will be notated as λ_{CO_2}. In order to use this wavelength subset, we should no longer use the PSG's output in units of transit depth, we must now use it in a more "raw" unit of spectral intensity, $\text{W/m}^2\text{/sr/µm}$. In this case, we will measure the quantity $\Delta F(\lambda) = F(\lambda)_{\text{pre transit}} - F(\lambda)_{\text{transit}}$. With signals in units of spectral intensity, we can more easily perform complex analysis on the

signals. Using this subset, the signals can be summed using the equation

$$\bar{D}_{\mathrm{CO_2}} = \frac{\sum_{\lambda_{\mathrm{CO_2}}} \Delta F(\lambda_{\mathrm{CO_2}})}{\sum_{\lambda_{\mathrm{CO_2}}} F(\lambda)_{\text{pre transit}}}, \tag{5.1}$$

where $\bar{D}_{\mathrm{CO_2}}$ is the average transit depth over the range of wavelengths where CO_2 is significant. The underlying goal of this method is to improve the overall signal to noise by summing across wavelengths. Very little information is lost using this method. Although "micro-features" in the spectra will disappear, this isn't an issue because they were already immeasurable due to the high noise.

With a solidly defined technique for measuring a signal, $\bar{D}_{\mathrm{CO_2}}$, we must now consider how the noise will be affected by this calculation. The noise results returned by the PSG don't consider some sources of noise. Other softwares like PandExo incorporate more sources of noise (Batalha et al., 2017), but the results returned by the PSG are still useful as they provide a lower limit on the noise. The noise before and during the transit will be similar to the point that they are indistinguishable, so a single noise function $N(\lambda)$ will be used to describe all measurements. Noise is also a function of exposure count and exposure time. The values used here will be the noise for a single transit, but the error should decrease from this according to the rule $N(\lambda) \propto 1/\sqrt{t}$ where t is the exposure time. In order to compute the error in $\bar{D}_{\mathrm{CO_2}}$, we need to go through step by step. The numerator uses subtraction, and the errors are the same magnitude, so the numerator's error is simply root two the original error. For the fraction, the numerator is much smaller than the denominator, and their errors are of similar magnitude, so the fractional error is approximately the fractional error in the numerator. The error in $\bar{D}_{\mathrm{CO_2}}$ is therefore given by the equation

$$\delta\bar{D}_{\mathrm{CO_2}} = \bar{D}_{\mathrm{CO_2}} \left| \frac{\sqrt{2}\delta F(\lambda)}{F(\lambda)} \right|, \tag{5.2}$$

where the absolute value implies adding each wavelength bin in quadrature, hence resolving the dependence on wavelength.

$\bar{D}_{\mathrm{CO_2}}$ and $\bar{D}_{\mathrm{H_2O}}$ are directly observable values, and similar values could be computed for other

species like CH_4 and O_3 if future models can incorporate them. $\bar{D}$ is an interesting measurement, but a question remains, what can it tell us about an exoplanet? To determine this, the ensemble of climate models must be used, and their values for $\bar{D}$ cross-referenced. As to how to might impact the value, the answer is non-trivial. It is certainly possible that surface temperature, surface pressure, partial pressures of the relevant species, or any number of other factors could be significant. The ensemble of climate models have different values for all these parameters, and they can be cross-referenced with the computed values of $\bar{D}$, to determine which values are significant. The simplest method of determining correlation is using the r^2 method, which will be used in this case. Table 5.1 computes the significance of different atmospheric parameters on $\bar{D}$. The only parameter strongly correlated with $\bar{D}$ is the surface temperature. All other parameters prove insignificant. Surprisingly, $\bar{D}_{CO_2}$ proves unreliable at measuring the partial pressure of CO_2. These results match the simple prediction that the most significant attribute in the transit depth is the overall height of the atmosphere. A high surface temperature will produce a high atmospheric scale height, which will lead to a larger transit depth. Unfortunately, it means that simply measuring $\bar{D}$ is not an effective method of identifying the abundance of certain species in an atmosphere. Although the presence of a feature like a spike at 15 micrometer would indicate the presence of CO_2, it alone cannot be used to measure the abundance.

The relationship between surface temperature and $\bar{D}$ can be visually seen in Figure 5.3. In this case, the 1σ noise after 10 transits is shown. Often NIRSpec produces lower noise, and H_2O produces stronger signals because it is present in more wavelengths across the spectrum. These results show errors low enough, that one could reasonably back out a surface temperature if given a value for $\bar{D}$. Unfortunately, as suggested in Table 5.1, no similar graphs could be produced for dependences on other atmospheric parameters.

For the wavelengths used to measure $\bar{D}_{CO_2}$ in MIRI, the 1σ error found by the PSG is 85.8 ppm after 1 transit. It is worth noting that since the PSG likely underestimates the total noise, the error is even larger. Even the most prominent features in the spectra are only 100 ppm tall. Some features like 15 micrometer CO_2 and 6 micrometer H_2O produce approximately 100 ppm gaps, as

Parameter	Instrument	Species Measured	r^2
Surface Temperature	NIRSpec	CO_2	0.834
		H_2O	0.757
	MIRI	CO_2	0.881
		H_2O	0.821
Surface Pressure	NIRSpec	CO_2	0.496
		H_2O	0.593
	MIRI	CO_2	0.563
		H_2O	0.650
N_2 Partial Pressure	NIRSpec	CO_2	0.415
		H_2O	0.501
	MIRI	CO_2	0.456
		H_2O	0.528
CO_2 Partial Pressure	NIRSpec	CO_2	0.036
		H_2O	0.034
	MIRI	CO_2	0.060
		H_2O	0.066

Table 5.1: Correlation Coefficients of Atmospheric Parameters and $\bar{D}$. Some of the most scientifically significant planetary attributes are shown in the left column. Their contribution to the transit depth is shown in the right column, where a number close to 1 indicates a strong correlation and a number close to 0 indicates a weak correlation. Both atmospheric species (implying a different set of wavelengths) and instrument will impact the transit depth, and therefore produce different r^2 values. Surface temperature has a strong correlation to the transit depth for both CO_2 and H_2O, but all others have weak or no correlation.

shown in Figure 5.2, but those signals are only that large for a few wavelengths, and the values of $\bar{D}$ would produce lower values, with better signal to noise. Overall, this is producing a rather bleak picture for detecting atmospheric parameters such as partial pressures of species or surface pressure. However, it is possible that when JWST launches, observed spectra can be compared with these model results to produce more accurate conclusions. Even though some measurements of $\bar{D}$ proved weak across models, they produced strong signals relative to the same models with missing atmospheric species. When JWST launches and spectra is actually collected, these techniques which can now only be tested on models will likely prove to be useful first steps in observation analysis.

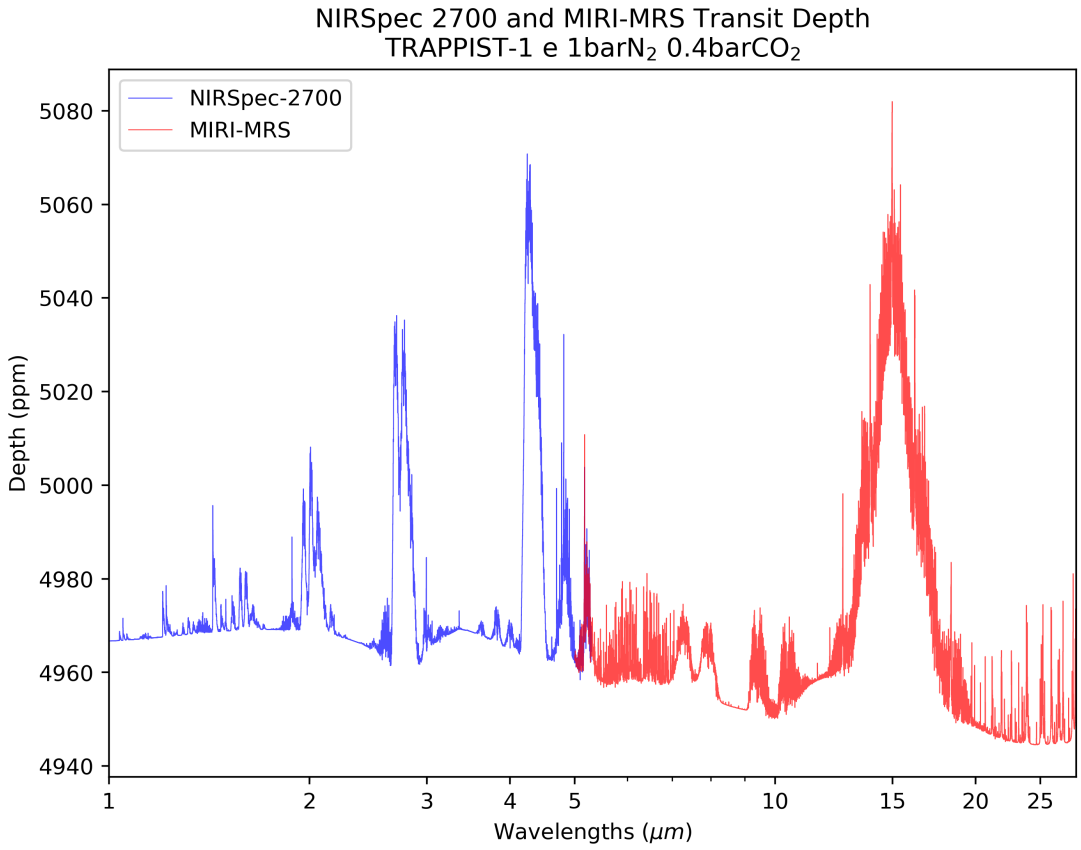

Figure 5.1: Transit spectra of NIRSpec-2700 and MIRI-MRS. In this spectra, there are a number of interesting absorption features. The widest feature is the 15 µm CO_2 absorption, which is both the widest and highest feature. Another distinguished feature is the 6 µm series of thin lines, which is due to H_2O. The logarithmic axis showed a more balanced spectra showing both the NIRSpec and MIRI instruments. Otherwise, the spectra would be dominated entirely by MIRI.

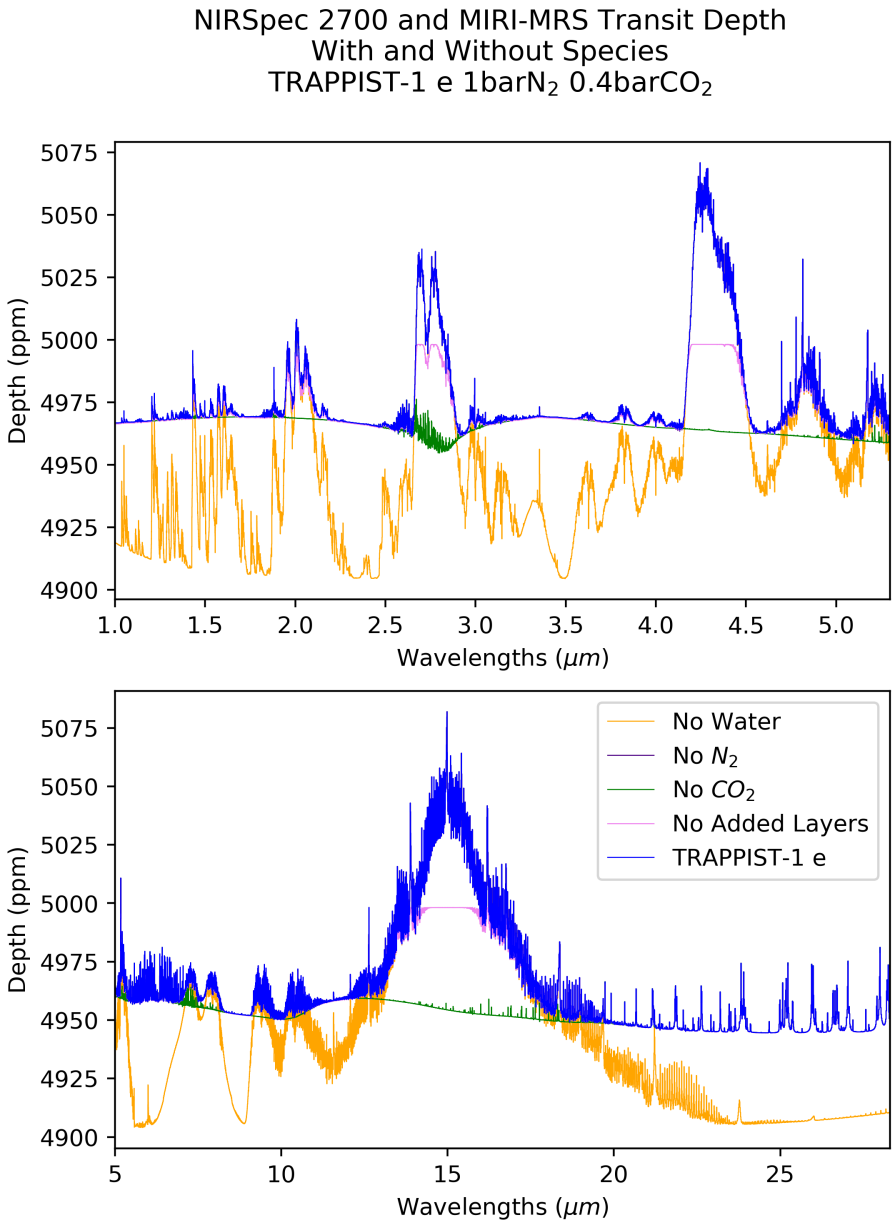

Figure 5.2: Transit Spectra Without Species. The top diagram is the NIRSpec transit and the bottom is the MIRI transit. Each color represents a different PSG simulation, where a different atmospheric species was zeroed-out before being sent to the PSG. The models are plotted in reverse order of the legend, with the normal transit on the top. The model without N_2 completely overlaps the blue plot because N_2 doesn't absorb in the infrared. Others only absorb at specific wavelengths, which is where the colors are visible.

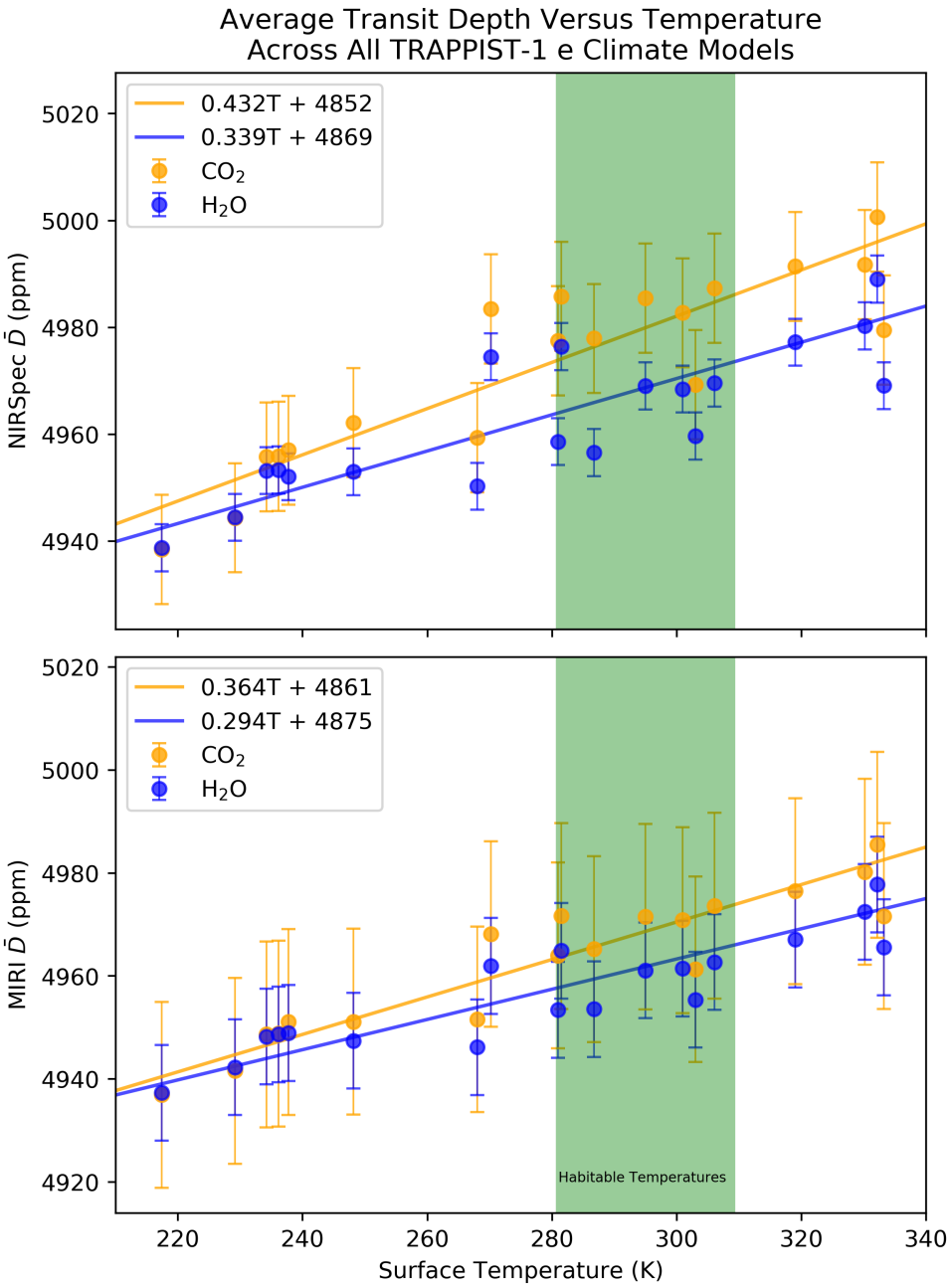

Figure 5.3: Transit Depth Versus Surface Temperature. Blue points are measurements of $\bar{D}_{H_2O}$, red points are measurements of $\bar{D}_{CO_2}$. Given the error bars on these points, it is hard to justify anything more than a linear fit between temperature and $\bar{D}$. Across both instruments, CO_2 has a steeper slope than H_2O, implying that it would be a better wavelength range to use when trying to determine surface temperature.

Chapter 6

Thermal Phase Curves

Although transits are useful, particularly for determining atmospheric species, they tell little about how the surface of a planet may look. Transits can only see the terminator profile, and would therefore only see a small section of the total atmosphere. In order to push our understanding of exoplanets, we would ideally like a method to measure an atmosphere across the planet instead of in a thin terminator. With this goal in mind, measuring the thermal emission of an exoplanet directly sounds like a promising technique. The most reliable way of doing this is by measuring the change in the thermal emission over time. For all transiting exoplanets, their surface will rotate relative to an observer. In Chapter 3, we found that there was significant structure to the atmosphere as well as significant variability over longitude. Therefore, thermal phase curves merit serious consideration as an observational technique for probing exoplanetary atmospheres.

In order to examine an exoplanetary atmosphere's thermal emission, we must first chose which wavelengths to examine. To first order, assuming that the host star and exoplanet emit as a blackbody, the ratio between the thermal emission of the two will always increase towards longer wavelengths. This can be confirmed by using the PSG. Using a global disk average for each phase, in increments of 5 deg, the PSG can be run, producing different signals at different points in an exoplanet's year. Some wavelengths do not experience strong temporal variability over time. To determine which wavelengths produce strong signals, we can compute $F_{\max} - F_{\min}$, which is shown in Figure 6.1. Longer wavelengths will change dramatically across phase, up to 80 ppm, while shorter wavelengths will change very little because the light in the shorter wavelengths is dominated

by the host star. The longest wavelengths vary more dramatically than the transit spectra with and without species in Figure 5.2. The variability in thermal emission changes dramatically, even between individual wavelengths. This is due to the molecular behavior of atmospheric species across different temperatures, primarily H_2O.

According to Figure 6.1, the most optimal wavelengths for thermal phase curve analysis are longer wavelengths, primarily to the right of the 17 µm jump, although wavelengths as short as 10 µm should be considered in the interest of reducing noise, although it would also reduce the magnitude of the signal by including lower values. Similar to transits, a subset of wavelengths can be defined such that

$$\frac{F_{\max}(\lambda) - F_{\min}(\lambda)}{F_*}(\lambda) \geq 8\,\text{ppm}, \tag{6.1}$$

but this will not prove as useful here as it did for transits because a number of these features in Figure 6.1 are extremely thin, and so reliably binning those values is impractical. In this case, $\lambda \geq 17\,\mu\text{m}$ will prove to be the most reliable method because of its simplicity, while other techniques don't provide much advantage for their added complexity.

In a thermal phase curve like the one shown in Figure 6.2, the shape is roughly the same across all wavelengths of any fixed climate model, and the phase of the steepest slope is highly dependent on which model is being simulated. The magnitude of this jump is dependent on the wavelength range examined. Including more wavelengths in the summation will improve signal to noise, but reduce the magnitude of the jump. The longest wavelengths produce the strongest jumps, but they also have the largest noise. Unlike transit spectra, where the different models would only produce mildly different results, a thermal phase curve produces varied results across models.

The most exciting result from Figure 6.2 is that the most habitable model of 1 bar N_2 0.4 bar CO_2 stands out distinctly from the other models both in the location of its steep rise and the shape of its gradual decline. This suggests that thermal phase curves would be the most likely technique to

distinguish between a habitable exoplanet with a stable atmosphere and an uninhabitable exoplanet.

Unfortunately, thermal phase curves using spectrographs on JWST are plagued with noise, the results shown in Figure 6.2 produced a noise of 407ppm, which far outweighs any signal. However, this technique isn't optimized for spectroscopy. For transits, it is advantageous to use spectroscopy as it can identify many interesting emission features from different molecular species, but in this case, there are no specific features to identify, so there is no disadvantage to using a long-wavelength filter and a CCD. MIRI also has an imaging instrument on it, with two filters that would be useful for this purpose, F2100W and F2550W, but the F2550W filter is the most obvious candidate because it operates at the longest wavelengths JWST can probe. Although the PSG is a tool designed primarily for the purposes of simulating spectrograph, a high resolution spectra is still useful for predicting broadband photometry measurements as photometry depends on the filters used and therefore the wavelengths probed.

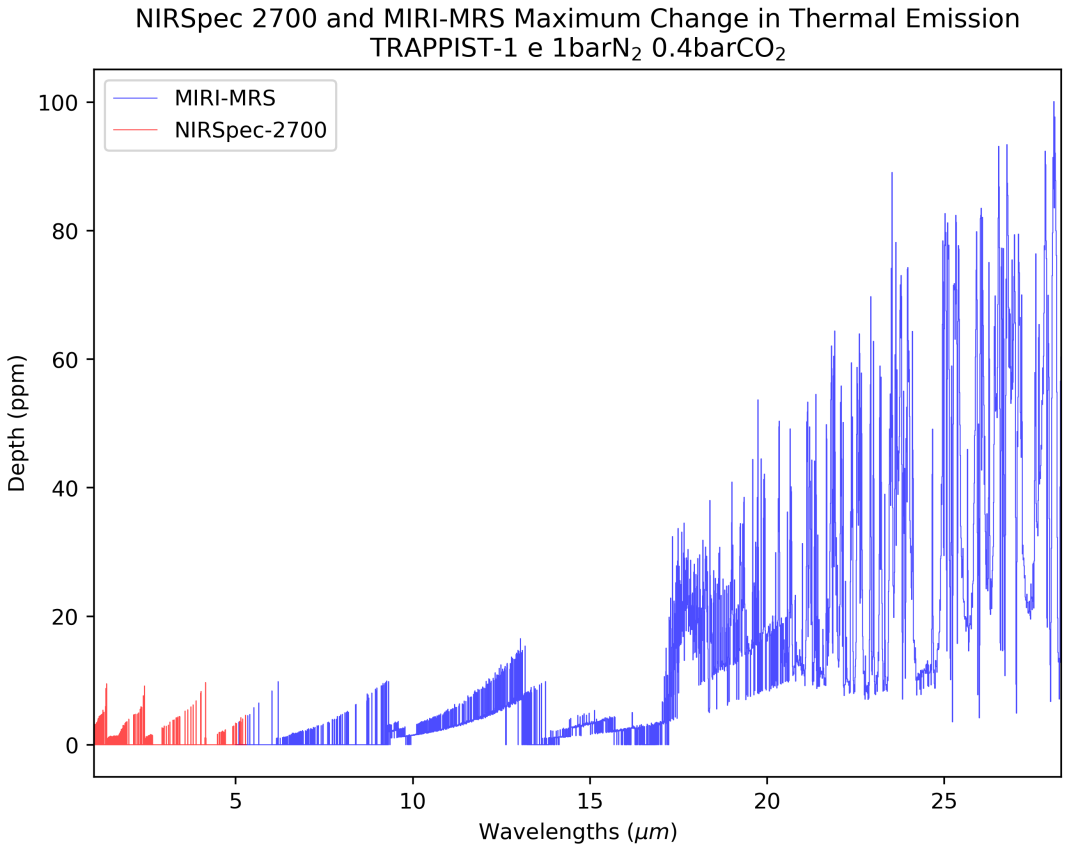

Figure 6.1: Maximum Change of Thermal Emission Over Time. NIRSpec and MIRI are shown together, and the y axis is the maximum thermal emission minus the minimum thermal emission. This technique demonstrates that longer wavelengths will experience stronger variability in thermal emission over time.

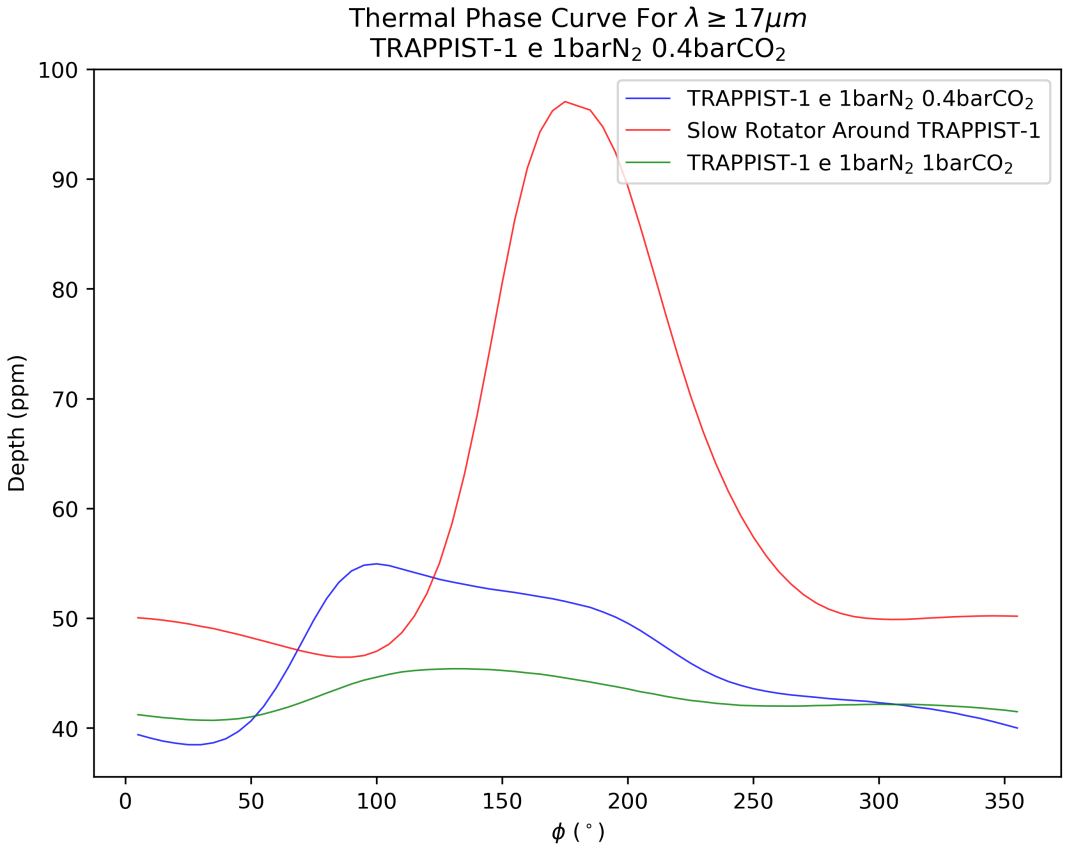

Figure 6.2: Thermal Phase Curve of TRAPPIST-1 e. The x axis here is orbital phase, but this value is linearly correlated with time. 0° is correlated with an occultation and 180° is correlated with a transit. However, both of those points were excluded from the plotted results because those values were discontinuous with the trend. The steep climb is from when the cloud-free areas rotate out of view toward Earth, and the gradual decline is where the night side rotates out of view, and eventually bottoms out when the substellar cloud is in view. Even if these features about the surface weren't known, this data could be used to infer the distribution of clouds on the surface. The red case, using the same climate model from Figure 3.4 is highly symmetric because the cloud distribution is highly symmetric. The hot case with 1 bar N_2 1 bar CO_2 is so low because there are little to no clouds like in the temperate case, so the thermal phase curve is virtually flat. If shorter wavelengths than 17 µm were included in this, they would produce the same shape, but the overall thermal phase curve will be over a smaller magnitude.

Chapter 7

Conclusion

Although JWST is the most powerful infrared telescope to date, and its ability to probe the mid-infrared greatly exceeds previous telescopes, exoplanetary spectroscopy struggles to overcome the noise. Using aggressive binning, these issues can be overcome, and the PSG in conjunction with climate models can be very useful in determining how to effectively bin the spectra to maximize specific signals. However, this technique as it was used here failed to measure the abundance of the atmospheric species CO_2 and H_2O. This does not imply that such a measurement is impossible, but other analysis techniques will be necessary to produce a meaningful measurement. In the wavelength ranges used here, transit spectra can be a reasonably reliable measure of surface temperature, and therefore habitability, and in 10 transits or less, the noise can be reasonably controlled for this purpose.

Transit spectroscopy suffers from some inherent limitations, such as it can only probe the terminator profile, and is therefore most useful for well-mixed atmospheric species only. Other atmospheric parameters like clouds are difficult to see in spectra, and it is not the most useful technique for those objectives.

If we wish to completely understand the behavior of a planet, we must use as many unique observational techniques as possible because each will provide different insights. In this effort, thermal phase curves are a promising technique, and they are the only method capable of analyzing an exoplanet's cloud distribution. Thermal phase curves also produce dramatically different signals depending on whether the planet is a fast rotator, a slow rotator, or too hot to sustain life. However,

more studies need to be done on different cases to fully understand the relationship between thermal phase curve shape and the atmosphere being probed. 3D climate models and the PSG are two useful tools, especially when used together.

The optimal wavelengths for thermal phase curves are the longest wavelengths, particularly past 17µm, which is well suited to the F2550W and F2100W filters on JWST. Even the most optimistic estimates of MIRI's spectral resolution show that thermal phase curves are not not well suited for a spectrograph as the signal to noise ratios are far too low. Unfortunately, the PSG is not designed to estimate signal to noise of MIRI's imaging instruments, so other tools would need to be used to estimate the signal to noise in those cases.

Thermal phase curves will be far more complicated on exoplanetary systems with more than one planet, which is the case for TRAPPIST-1. Although the results here show promise for the technique of thermal phase curves, the process of implementing this technique in a observation would involve computing thermal phase curves for multiple planets at once. This can be overcome with advanced reduction algorithms, and the PSG with 3D climate models would likely serve as a useful tool for matching the data to an atmosphere. Thermal phase curves would be most fruitful in single-planet systems near the habitable zone, as they were implemented here.

As exoplanetary astrophysics evolves over the next few years, the need for accurate climate models will only increase. Climate models are the only way we can effectively understand and predict an exoplanet's atmosphere, and so far, tidally locked exoplanet atmospheres have been dramatically different from what we would have expected from Earth's atmosphere. The climate models used here are extremely probative, but they are missing many features that will likely be important on an exoplanet. The presence of atmospheric species like O_3, CH_4, and others are important additions to future models, as well as the integration of M-dwarf solar physics like stellar flares, which will likely be a major source of atmospheric loss. Carefully integrating these features into existing climate models will greatly improve the probative value of climate models, particularly when used with the PSG to integrate them into spectra simulations. The probative potential of climate models in conjunction with the PSG goes far beyond the results discussed in this paper, and

together they serve as a great technique for furthering our understanding of potentially habitable worlds.

References

2018, James Webb Space Telescope, Tech. rep., Goddard Space Flight Center

2019, NASA Exoplanet Archive, https://exoplanetarchive.ipac.caltech.edu/

Afrin Badhan, M., Wolf, E. T., Kopparapu, R. K., et al. 2019, arXiv e-prints, arXiv:1902.04086. https://arxiv.org/abs/1902.04086

Batalha, N. E., Mandell, A., Pontoppidan, K., et al. 2017, Publications of the Astronomical Society of the Pacific, 129, 064501, doi: 10.1088/1538-3873/aa65b0

Cowan, N. B., & Agol, E. 2008, ApJL, 678, L129, doi: 10.1086/588553

Delrez, L., Gillon, M., Triaud, A. H. M. J., et al. 2018, MNRAS, 475, 3577, doi: 10.1093/mnras/sty051

Ducrot, E., Sestovic, M., Morris, B. M., et al. 2018, AJ, 156, 218, doi: 10.3847/1538-3881/aade94

E Walter, M. 2010, Notices ofthe maerican Mathematical Society, 57

Fortelli, A., Scafetta, N., & Mazzarella, A. 2016, Atmospheric Environment, 143, 218 , doi: https://doi.org/10.1016/j.atmosenv.2016.08.050

Fortney, J., Kataria, T., Stevenson, K., et al. 2018, arXiv e-prints, arXiv:1803.07730. https://arxiv.org/abs/1803.07730

Gillon, M., Triaud, A. H. M. J., Demory, B.-O., et al. 2017, Nature, 542, 456, doi: 10.1038/nature21360

Haqq-Misra, J., Wolf, E. T., Joshi, M., Zhang, X., & Kopparapu, R. K. 2018, ApJ, 852, 67, doi: 10.3847/1538-4357/aa9f1f

Jenkins, J. M., Twicken, J. D., Batalha, N. M., et al. 2015, AJ, 150, 56, doi: 10.1088/0004-6256/150/2/56

Kite, E. S., & Ford, E. B. 2018, The Astrophysical Journal, 864, 75

Koll, D. D. B., & Abbot, D. S. 2015, The Astrophysical Journal, 802, 21

Konacki, M., Torres, G., Jha, S., & Sasselov, D. D. 2003, Nature, 421, 507

Kopparapu, R. k., Wolf, E. T., Arney, G., et al. 2017, ApJ, 845, 5, doi: 10.3847/1538-4357/aa7cf9

Latham, D. W., Mazeh, T., Stefanik, R. P., Mayor, M., & Burki, G. 1989, Nature, 339, 38, doi: 10.1038/339038a0

Leconte, J., Wu, H., Menou, K., & Murray, N. 2015, Science, 347, 632, doi: 10.1126/science.1258686

Mullally, F., Thompson, S. E., Coughlin, J. L., Burke, C. J., & Rowe, J. F. 2018, AJ, 155, 210, doi: 10.3847/1538-3881/aabae3

Neale, R. B., Chen, C., & Gettelman, A. 2012

Newton, S. I. 1846, Mathematical Principles of Natural Philosophy

Ricker, G. R., Winn, J. N., Vanderspek, R., et al. 2014, 9143, 914320, doi: 10.1117/12.2063489

Traub, W. A. 2012, The Astrophysical Journal, 745, 20

Turbet, M., Bolmont, E., Leconte, J., et al. 2018, A&A, 612, A86, doi: 10.1051/0004-6361/201731620

Villanueva, G. L., Smith, M. D., Protopapa, S., Faggi, S., & Mandell, A. M. 2018, JQSRT, 217, 86, doi: 10.1016/j.jqsrt.2018.05.023

von Essen, C., Mallonn, M., Welbanks, L., et al. 2018, arXiv e-prints, arXiv:1811.02573. https://arxiv.org/abs/1811.02573

Wang, J., Zhang, L., & Dai, A. 2005, Journal of Geophysical Research: Atmospheres, 110, doi: 10.1029/2005JD006215

Way, M. J., Del Genio, A., & Amundsen, D. S. 2018, arXiv e-prints, arXiv:1802.05434. https://arxiv.org/abs/1802.05434

Wolf, E. T. 2017, ApJ, 839, L1, doi: 10.3847/2041-8213/aa693a

Wolf, E. T. 2018, The Astrophysical Journal Letters, 855, L14

Wolf, E. T., Shields, A. L., Kopparapu, R. K., Haqq-Misra, J., & Toon, O. B. 2017, ApJ, 837, 107, doi: 10.3847/1538-4357/aa5ffc

Yang, J., Abbot, D. S., Koll, D. D. B., Hu, Y., & Showman, A. P. 2019, ApJ, 871, 29, doi: 10.3847/1538-4357/aaf1a8

Appendix A

Project Code

In the creation of this thesis, over 2000 lines of code were written. In the interest of academic transparency and review, this code is made public and free to anyone interested in reviewing it. All work was done in Python 3.6, either as a library or via Jupyter Notebooks. The main data pipeline is contained in PSG.py, while the analysis and figures were created in Jupyter Notebooks, and can be reproduced interactively there.

All the project code is available on a GitHub repository, which can be found at `https://github.com/StarkillerX42/GatlinPSG`. The results produced here would require the climate models produced by Eric Wolf, which are also publicly available at `https://archive.org/details/TRAPPIST-1_3D_Climate_Simulations`.